
A Mini-Block Natural Gradient Method for Deep Neural Networks

Achraf Bahamou¹ Donald Goldfarb¹ Yi Ren¹

Abstract

Currently, the training of deep neural networks (DNNs) is mostly done using first-order methods. Some of these methods (e.g., Adam, AdaGrad, and RMSprop, and their variants) incorporate a small amount of curvature information by using a diagonal matrix to precondition the stochastic gradient. Recently, effective second-order methods, such as KFAC, K-BFGS, Shampoo, and TNT, have been developed for training DNNs, by preconditioning the stochastic gradient by layer-wise block-diagonal matrices. Here we propose and analyze the convergence of an approximate natural gradient method, mini-block Fisher (MBF), that lies in between these two classes of methods. Specifically, our method uses a block-diagonal approximation to the Fisher matrix, where for each DNN layer, whether it is convolutional or feed-forward and fully connected, the associated diagonal block is also block-diagonal and is composed of a large number of mini-blocks of modest size. Our novel approach utilizes the parallelism of GPUs to efficiently perform computations on the large number of matrices in each layer. Consequently, MBF’s per-iteration computational cost is only slightly higher than it is for first-order methods. Finally, MBF’s performance is compared to that of several baseline methods, on both Auto-encoder and CNN problems, to validate its effectiveness both in terms of time efficiency and generalization power.

1. Introduction

First-order methods based on stochastic gradient descent (SGD) (Robbins & Monro, 1951), and in particular, the class of adaptive learning rate methods, such as AdaGrad (Duchi et al., 2011), RMSprop (Hinton et al., 2012), and Adam (Kingma & Ba, 2014), are currently the most widely used methods to train deep learning models (the recent paper (Schmidt et al., 2021) lists 65 methods that have “Adam” or “Ada” as part of their names). While these methods are easy to implement and have low computational complexity, they make use of only a limited amount of curvature information. Standard SGD and its mini-batch variants, use none. SGD with momentum (SGD-m) (Polyak, 1964) and stochastic versions of Nesterov’s accelerated gradient method (Nesterov, 1998), implicitly make use of curvature by choosing step directions that combine the negative gradient with a scaled multiple of the previous step direction, very much like the classical conjugate gradient method.

To effectively optimize ill-conditioned functions, one usually needs to use second-order methods, which range from the classical Newton method to those that use approximations to the Hessian matrix, such as BFGS quasi-Newton methods (Broyden, 1970; Fletcher, 1970; Goldfarb, 1970; Shanno, 1970), including limited memory variants (Liu & Nocedal, 1989), and Gauss-Newton methods (Ortega & Rheinboldt, 1970). To handle large data sets that arise in solving machine learning problems, variants of these methods such as sub-sampled Newton (Xu et al., 2019), stochastic quasi-Newton (Byrd et al., 2016; Gower et al., 2016; Wang et al., 2017), Gauss-Newton (GN) and natural gradient (NG) (Amari et al., 2000), Hessian-free (Martens, 2010), and Krylov subspace methods (Vinyals & Povey, 2012) have been developed. However, in all of these second-order methods, whether they use the Hessian or an approximation to it, the size of the matrix becomes prohibitive when the number of training parameters is huge.

¹Department of Industrial Engineering and Operations Research, Columbia University, New York NY, USA. Correspondence to: Achraf Bahamou <ab4689@columbia.edu>.

Therefore, deep learning training methods have been proposed that use layer-wise block-diagonal approximations to the second-order preconditioning matrix. These include a Sherman-Morrison-Woodbury based variant (Ren & Goldfarb, 2019) and a low-rank variant (Roux et al., 2008) of the block-diagonal Fisher matrix approximations for NG methods. Also, Kronecker-factored matrix approximations of the diagonal blocks in Fisher matrices have been proposed to reduce the memory and computational requirements of NG methods, starting from KFAC for multilayer perceptrons (MLPs) (Martens & Grosse, 2015), which was extended to CNNs in (Grosse & Martens, 2016); (in addition, see Heskes (2000); Povey et al. (2014); George et al. (2018)).

Kronecker-factored QN methods (Goldfarb et al., 2020), generalized GN methods (Botev et al., 2017), an adaptive block learning rate method Shampoo (Gupta et al., 2018) based on AdaGrad, and an approximate NG method TNT (Ren & Goldfarb, 2021b), based on the assumption that the sampled tensor gradient follows a tensor-normal distribution have also been proposed.

2. Our Contributions

In this paper, we propose a brand new approximate natural gradient *Mini-Block Fisher* method (MBF) that lies in between adaptive first order methods and block diagonal approximate second-order methods. Specifically, MBF uses a block-diagonal approximation to the Fisher matrix, where for each layer in the DNN, whether it is convolutional or feed-forward and fully-connected, the associated diagonal block is also block-diagonal and is composed of a large number of mini-blocks of modest size.

Crucially, MBF has comparable memory requirements to those of first-order methods, while its per-iteration time complexity is smaller, and in many cases, much smaller than that of popular second-order methods (e.g. KFAC) for training DNNs. Further, we prove convergence results for a variant of MBF under relatively mild conditions.

In numerical experiments on well-established Autoencoder and CNN models, MBF consistently outperformed state-of-the-art (SOTA) first-order methods (SGD-m and Adam) and performed favorably compared to popular second-order methods (KFAC and Shampoo).

3. Notation and Definitions

Notation. The following notation is used throughout the paper: $[L] := \{1, \dots, L\}$, $\text{Diag}_{i \in [L]}(A_i)$ is the block diagonal matrix with matrices $\{A_1, \dots, A_L\}$ on its diagonal; $\mathbf{X} \in \mathbb{R}^{n \times d}$ is the input data, i.e. $\mathbf{X} = [x_1, \dots, x_n]^\top$. $\lambda_{\min}(M)$, $\lambda_{\max}(M)$ are the smallest and largest eigenvalues of the matrix M ; the Kronecker product by \otimes ; $\|\cdot\|_2$ denotes the Euclidean norm of a vector or matrix; and $\text{vec}(A)$ is the operator that vectorizes A by stacking its columns.

We consider a DNN with L layers, defined by weight matrices W_l , for $l \in [L]$, that transforms the input vector \mathbf{x} to an output $f(\mathbf{W}, \mathbf{x})$. For a data-point (x, y) , the loss $\ell(f(\mathbf{W}, \mathbf{x}), y)$ between the output $f(\mathbf{W}, \mathbf{x})$ of the DNN and y is a non-convex function of the vector $\mathbf{W} = [\text{vec}(W_1)^\top, \dots, \text{vec}(W_L)^\top]^\top \in \mathbb{R}^p$, containing all of the network’s parameters, and ℓ measures the accuracy of the prediction (e.g. squared error loss, cross entropy loss). The optimal parameters are obtained by minimizing the average loss \mathcal{L} over the training set:

$$\mathcal{L}(\mathbf{W}) = \frac{1}{n} \sum_{i=1}^n \ell(f(\mathbf{W}, \mathbf{x}_i), \mathbf{y}_i), \quad (1)$$

This setting is applicable to most common models in deep learning such as MLPs, CNNs, recurrent neural networks (RNNs), etc. In these models, the trainable parameter W_l ($l = 1, \dots, L$) come from the weights of a layer, whether it be a feed-forward, convolutional, recurrent, etc. For the weight matrix $W_l \in \mathbb{R}^{p_l}$ corresponding to layer l and a subset of indices $b \subset \{1, \dots, p_l\}$, we denote by $W_{l,b}$, the subset of parameters of W_l corresponding to b .

The average gradient over a mini-batch of size m is defined as $\mathbf{g}^{(m)} = \frac{1}{m} \sum_{i=1}^m \frac{\partial \ell(f(\mathbf{W}, \mathbf{x}_i), \mathbf{y}_i)}{\partial \mathbf{W}}$, which is computed using standard back-propagation. In the full-batch case, where $m = n$, we have that $\mathbf{g}^{(n)} = \mathbf{g} = \frac{\partial \mathcal{L}(\mathbf{W})}{\partial \mathbf{W}}$. Here, we are using the notation $\mathcal{D}X := \frac{\partial \mathcal{L}(\mathbf{W})}{\partial X}$ for any subset of variables X of \mathbf{W} .

The Jacobian $\mathbf{J}(\mathbf{W})$ of the loss $\mathcal{L}(\cdot)$ w.r.t the parameters \mathbf{W} for a single output network is defined as $\mathbf{J} = [\mathbf{J}_1^\top, \dots, \mathbf{J}_n^\top]^\top \in \mathbb{R}^{n \times p}$, where \mathbf{J}_i^\top is the gradient of the loss w.r.t the parameters, i.e., $\mathbf{J}_i^\top = \text{vec}(\frac{\partial \ell(f(\mathbf{W}, \mathbf{x}_i), \mathbf{y}_i)}{\partial \mathbf{W}})$. We use the notation

$\mathbf{J}_i^{X^\top} = \text{vec}\left(\frac{\partial \ell(f(\mathbf{W}, \mathbf{x}_i), \mathbf{y}_i)}{\partial \mathbf{X}}\right)$ and $\mathbf{J}^X = [\mathbf{J}_1^{X^\top}, \dots, \mathbf{J}_n^{X^\top}]^\top$ for any subset of variables X of \mathbf{W} .

The Fisher matrix $\mathbf{F}(\mathbf{W})$ of the model's conditional distribution is defined as

$$\mathbf{F}(\mathbf{W}) = \mathbb{E}_{\substack{x \sim Q_x \\ y \sim p_{\mathbf{W}}(\cdot|x)}} \left[\frac{\partial \log p_{\mathbf{W}}(y|x)}{\partial \mathbf{W}} \left(\frac{\partial \log p_{\mathbf{W}}(y|x)}{\partial \mathbf{W}} \right)^\top \right],$$

where Q_x is the data distribution of x and $p_{\mathbf{W}}(\cdot|x)$ is the density function of the conditional distribution defined by the model with a given input x . As shown in (Martens, 2020), the Fisher matrix is equivalent to the Gauss-Newton matrix if the conditional distribution is in the exponential family, such as a categorical distribution for classification or a Gaussian distribution for regression. Therefore, in such cases, the Fisher matrix can be compactly written as:

$$\begin{aligned} \mathbf{F}(\mathbf{W}) &= \frac{1}{n} \sum_{i=1}^n \frac{\partial \ell(f(\mathbf{W}, \mathbf{x}_i), \mathbf{y}_i)}{\partial \mathbf{W}} \frac{\partial \ell(f(\mathbf{W}, \mathbf{x}_i), \mathbf{y}_i)}{\partial \mathbf{W}}^\top \\ &= \frac{1}{n} \mathbf{J}(\mathbf{W})^\top \mathbf{J}(\mathbf{W}) \end{aligned}$$

We denote by $\mathbf{F}^X = \frac{1}{n} (\mathbf{J}^X)^\top \mathbf{J}^X$, the sub-block of $\mathbf{F}(\mathbf{W})$ associated with any subset of variables $X \subset \mathbf{W}$, and write $(\mathbf{F}^X)^{-1}$ as \mathbf{F}_X^{-1} .

Natural gradient descent (NGD). At each iteration, NGD preconditions the gradient direction by the inverse of the damped Fisher Information Matrix (FIM) as follows:

$$\mathbf{W}(k+1) = \mathbf{W}(k) - \alpha (\mathbf{F}(\mathbf{W}(k)) + \lambda \mathbf{I})^{-1} \mathbf{g}(k), \quad (2)$$

where α is the learning rate and λ is the damping parameter.

4. Mini-block Fisher (MBF) method

In order to overcome the computational bottleneck of computing and storing the inverse of the $p \times p$ damped FIM, $(\mathbf{F} + \lambda \mathbf{I})^{-1}$, where p can be in the millions, we assume, as in KFAC and Shampoo, that the Fisher matrix has a block diagonal structure, where the l_{th} diagonal block l corresponds to the covariance of the gradient of the model w.r.t to the weights in the l_{th} layer. Hence, the approximate Fisher matrix is:

$$\mathbf{F}(\mathbf{W}) \approx \text{Diag}(\mathbf{F}^{W_1}, \dots, \mathbf{F}^{W_L}).$$

Figure 1 summarizes how several existing methods further approximate these diagonal blocks.

Our proposed method MBF further approximates each of the diagonal blocks \mathbf{F}_{W_l} by a block-diagonal matrix, composed of a typically large number mini-blocks, depending on the nature of layer l , as follows:

4.1. Layer l is convolutional:

For simplicity, we assume that:

1. the convolutional layer l is 2-dimensional;
2. the layer has J input channels indexed by $j = 1, \dots, J$, and I output channels indexed by $i = 1, \dots, I$;
3. there are $I \times O$ kernels $W_{l,j,i}$, each of size $(2R+1) \times (2R+1)$, with spatial offsets from the centers of each filter indexed by $\delta \in \Delta := \{-R, \dots, R\} \times \{-R, \dots, R\}$;
4. the stride is of length 1, and the padding is equal to R , so that the sets of input and output spatial locations ($t \in \mathcal{T} \subset \mathbf{R}^2$) are the same.¹;

¹The derivations in this paper can also be extended to the case where the stride is greater than 1.

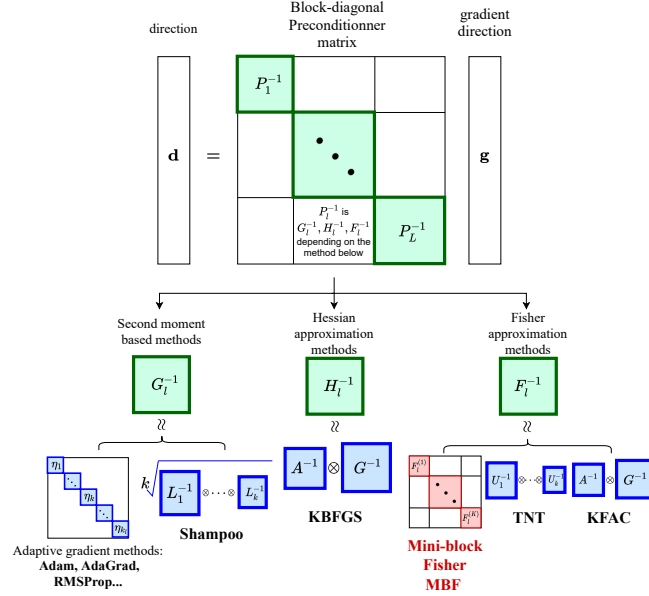


Figure 1: MBF vs other block-diagonal preconditioned gradient methods.

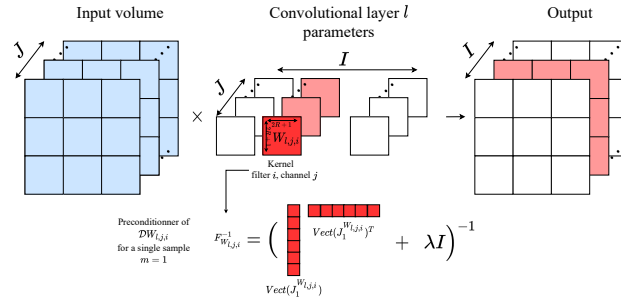


Figure 2: Illustration of MBF's approximation for a convolutional layer.

For such layers, we use the following $(IJ + 1) \times (IJ + 1)$ block-diagonal approximation to the l_{th} diagonal block \mathbf{F}^{W_l} of the Fisher matrix

$$\text{diag}\{\mathbf{F}^{W_{l,1,1}}, \dots, \mathbf{F}^{W_{l,1,I}}, \dots, \mathbf{F}^{W_{l,J,1}}, \dots, \mathbf{F}^{W_{l,J,I}}, \mathbf{F}^{b_l}\},$$

where each of the IJ diagonal blocks $\mathbf{F}^{W_{l,j,i}}$ is a $|\Delta| \times |\Delta|$ symmetric matrix corresponding to the kernel vector $W_{l,j,i}$ and where the diagonal block \mathbf{F}^{b_l} is an $I \times I$ diagonal matrix corresponding to the bias vector b_l . Therefore, the preconditioning matrix $F_{W_{l,j,i}}^{-1}$ corresponding to the kernel for input-output channel pair (j, i) is given by:

$$F_{W_{l,j,i}}^{-1} := \left(\frac{1}{n} (\mathbf{J}^{W_{l,j,i}})^T \mathbf{J}^{W_{l,j,i}} + \lambda \mathbf{I} \right)^{-1}$$

A common choice in CNNs is to use either a 3×3 or 5×5 kernel for all of the IJ channel pairs in a layer. Therefore, all of these matrices are of the same (small) size, $|\Delta| \times |\Delta|$, and can be inverted efficiently by utilizing the parallelism of GPUs. We illustrate MBF's approximation for a convolutional layer for the case of one data-point in Fig. 2.

4.2. Layer l is feed forward and fully connected (ff-fc)

For a ff-fc layer with I inputs and O outputs, we use the following $O \times O$ block-diagonal approximation to the Fisher matrix

$$\mathbf{F}^{W_l} \approx \text{diag}\{\mathbf{F}^{W_{l,1}}, \dots, \mathbf{F}^{W_{l,O}}\},$$

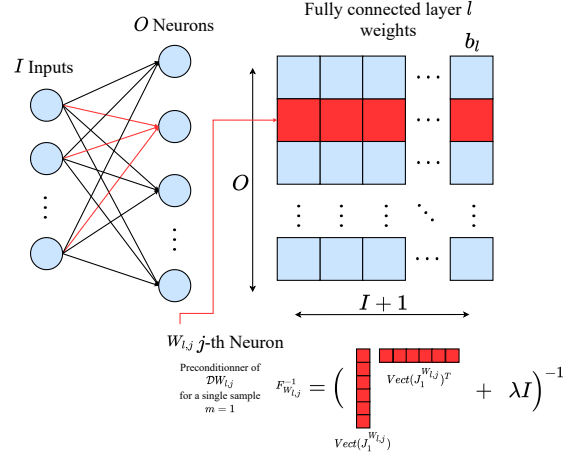


Figure 3: Illustration of MBF's preconditionner for a fully-connected layer.

whose j_{th} diagonal block $F^{W_{l,j}}$ is an $(I+1) \times (I+1)$ symmetric matrix corresponding to the vector $W_{l,j}$ of I weights from all of the input neurons and the bias to the j_{th} output neuron. Therefore, the preconditioning matrix $F_{W_{l,j}}^{-1}$ corresponding to the j_{th} output neuron is given by:

$$F_{W_{l,j}}^{-1} := \left(\frac{1}{n} (\mathbf{J}^{W_{l,j}})^T \mathbf{J}^{W_{l,j}} + \lambda I \right)^{-1}$$

Our choice of such a mini-block subdivision was motivated by the findings presented in (Roux et al., 2008), first derived in (Collobert, 2004), where it was shown that the Hessian of a neural network with one hidden layer with cross-entropy loss converges during optimization to a block-diagonal matrix, where the diagonal blocks correspond to the weights linking all the input units to one hidden unit and all of the hidden units to one output unit. This suggests that a similar block-diagonal structure applies to the Fisher matrix in the limit of a sequence of iterates produced by an optimization algorithm. Finally, since the O matrices $F^{W_{l,j}}$, for $j = 1, \dots, O$, are all of the same size, $(I+1) \times (I+1)$, they can be inverted efficiently by utilizing the parallelism of GPUs. We illustrate MBF's approximation for a fully connected layer for the case of one data-point in Figure 3.

Algorithm 1 Generic MBF training algorithm

Require: Given learning rates $\{\alpha_k\}$, damping value λ , batch size m

- 1: **for** $k = 1, 2, \dots$ **do**
 - 2: Sample mini-batch M of size m
 - 3: Perform a forward-backward pass over M to compute stochastic gradient $\mathcal{D}W_l$ ($l = 1, \dots, L$)
 - 4: **for** $l = 1, \dots, L$ **do**
 - 5: **for** mini-block b in layer l , **in parallel do**
 - 6: $F_{W_{l,b}}^{-1} := \left(\frac{1}{m} (\mathbf{J}^{W_{l,b}})^T \mathbf{J}^{W_{l,b}} + \lambda I \right)^{-1}$
 - 7: $W_{l,b} = W_{l,b} - \alpha_k F_{W_{l,b}}^{-1} \mathcal{D}W_{l,b}$
 - 8: **end for**
 - 9: **end for**
 - 10: **end for**
-

Algorithm 1 below gives the pseudo-code for a generic version of MBF. Since updating the Fisher mini-blocks is time consuming in practice as it requires storing and computing the individual gradients, we propose in Section 7 below, a practical approach for approximating these matrices. However, we first present empirical results that justify and motivate both the kernel-based and the all-to-one mini-block subdivisions described above for convolutional and ff-fc layers, respectively, followed by a discussion of the linear convergence of the generic MBF algorithm.

5. Motivation for MBF

Our choice of mini-blocks for both the convolutional and fully-connected feed-forward layers was motivated by the observation that most of the weight in the inverse of the empirical FIM resides in diagonal blocks, and in particular in the mini-blocks described above. More specifically, to illustrate this observation for convolutional layers, we trained a simple convolutional neural network, Simple CNN, (see Appendix B.5 for more details) on Fashion MNIST (Xiao et al., 2017). Figure 4 shows the heatmap of the absolute value of the inverse empirical FIM corresponding to the first convolutional layer, which uses 32 filters of size 5×5 (thus 32 mini-blocks of size 25×25). One can see that the mini-block (by filter) diagonal approximation is reasonable. Figures for the second convolutional layer are included in the Appendix B.5.

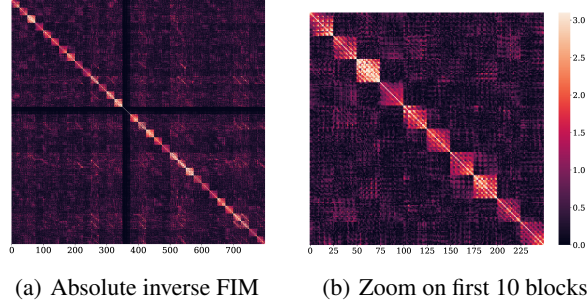


Figure 4: Absolute inverse of the empirical FIM after 10 epochs for the first convolutional layer of the Simple CNN network that uses 32 filters of size 5×5 .

Since the fully-connected feed-forward layers in the Simple-CNN model result in a FIM for those layers that is too large to work with, we chose to illustrate the mini-block structure of the FIM on a standard DNN, partially trained to classify a 16×16 down-scaled version of MNIST that was also used in (Martens & Grosse, 2015). Figure 5 shows the heatmap of the absolute value of the inverse empirical FIM for the last and middle fully connected layers (including bias). One can see that the mini-block (by neuron) diagonal approximation is reasonable. A bigger Figure for the second fully connected layer is included in Appendix B.5).

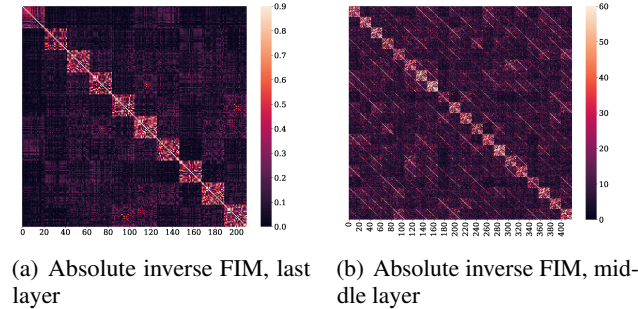


Figure 5: Absolute inverse of the empirical FIM after 50 epochs of the last and middle fully connected layers (including bias) of a 7-layer (256-20-20-20-20-10) feed-forward DNN using tanh activations, partially trained to classify a 16×16 down-scaled version of MNIST.

6. Linear Convergence

We follow the framework established in (Zhang et al., 2019a) to provide convergence guarantees for the idealized MBF with exact gradients (i.e. full batch case with $m = n$). We focus on the single output case with square error loss but a general case with multiple outputs will be similar.

We denote by $\mathbf{u}(\mathbf{W}) = [f(\mathbf{W}, x_1), \dots, f(\mathbf{W}, x_n)]^\top$ the output vector and $\mathbf{y} = [y_1, \dots, y_n]^\top$ the true labels. We consider

the squared error loss \mathcal{L} on a given data-set $\{x_i, y_i\}_{i=1}^n$ with $x_i \in \mathbb{R}^d$ and $y_i \in \mathbb{R}$, i.e. the objective is to minimize

$$\min_{\mathbf{W} \in \mathbb{R}^p} \mathcal{L}(\mathbf{W}) = \frac{1}{2} \|\mathbf{u}(\mathbf{W}) - \mathbf{y}\|^2.$$

The update rule of MBF with exact gradient becomes

$$\mathbf{W}(k+1) = \mathbf{W}(k) - \eta(\mathbf{F}_{MB}(\mathbf{W}(k)) + \lambda \mathbf{I})^{-1} \mathbf{J}(k)^\top (\mathbf{u}(\mathbf{W}(k)) - \mathbf{y}),$$

where $\mathbf{F}_{MB}(\mathbf{W}(k)) := \frac{1}{n} \mathbf{J}_{MB}(\mathbf{W}(k))^\top \mathbf{J}_{MB}(\mathbf{W}(k))$ is the mini-block-Fisher matrix and the mini-block Jacobian is defined as $\mathbf{J}_{MB}(k) = \text{Diag}_{l \in [L]} \text{Diag}_b(\mathbf{J}^{\mathbf{W}_{l,b}}(k))$ and

$$\mathbf{J}^{\mathbf{W}_{l,b}}(k) := \left[\frac{\partial \ell(f(\mathbf{W}(k), \mathbf{x}_1), \mathbf{y}_1)}{\partial \mathbf{W}_{l,b}}, \dots, \frac{\partial \ell(f(\mathbf{W}(k), \mathbf{x}_n), \mathbf{y}_n)}{\partial \mathbf{W}_{l,b}} \right]^\top$$

We use similar assumptions to those used in (Zhang et al., 2019a), where the first assumption, ensures that at initialization, the mini-block Gram matrices are all positive-definite, (i.e., the rows of their respective Jacobians are linearly independent), and the second assumption ensures the stability of the Jacobians by requiring that the network is close to a linearized network at initialization and therefore MBF's update is close to the gradient descent direction in the output space. These assumptions allow us to control the convergence rate.

Assumption 6.1. The mini-block Gram matrices $\mathbf{J}^{\mathbf{W}_{l,b}}(0) \mathbf{J}^{\mathbf{W}_{l,b}}(0)^\top$ at initialization are positive definite, i.e. $\min_{l \in [L]} \min_b \lambda_{\min}(\mathbf{J}^{\mathbf{W}_{l,b}}(0) \mathbf{J}^{\mathbf{W}_{l,b}}(0)^\top) = \lambda_0 > 0$.

Assumption 6.2. There exists $0 < C \leq \frac{1}{2}$ that satisfies $\|\mathbf{J}(\mathbf{W}(k)) - \mathbf{J}(\mathbf{W}(0))\|_2 \leq \frac{C}{3} \sqrt{\lambda_0}$ if $\|\mathbf{W}(k) - \mathbf{W}(0)\|_2 \leq \frac{3}{\sqrt{\lambda_0}} \|\mathbf{y} - \mathbf{u}(0)\|_2$.

We present our convergence result in Theorem 1.

Theorem 1. Suppose Assumptions 6.1, 6.2 hold. Consider the Generic BMF Algorithm 1, using exact gradients for a network with L layers. Then there exists an interval of suitable damping values λ in $[\underline{\lambda}, \bar{\lambda}]$ and corresponding small enough learning rates η_λ , such that for any learning rate $0 \leq \eta \leq \eta_\lambda$ we have $\|\mathbf{u}(\mathbf{W}(k)) - \mathbf{y}\|_2^2 \leq (1 - \eta)^k \|\mathbf{u}(\mathbf{W}(0)) - \mathbf{y}\|_2^2$.

Theorem 1 states that MBF converges to the global optimum with a linear rate under Assumptions 1 and 2. Our analysis is an adaptation of the proof in (Zhang et al., 2019a), where we first exploit Assumptions 6.1 and 6.2 to obtain a positive lower bound on the eigenvalues of MBF's Fisher-mini-block matrix $\mathbf{F}_{MB}(\mathbf{W}(k))$, which then allows us to characterize the rate of convergence of our method. The proof can be found in the Appendix A.

7. Implementation Details of MBF and Comparison on Complexity

Mini-batch averages, Exponentially decaying averages and Momentum

Because the size of training data sets is usually large, we use mini-batches to estimate the quantities needed for MBF. We use \bar{X} to denote the average value of X over a mini-batch for any quantity X . Moreover, for the Fisher mini-blocks, we use moving averages to both reduce the stochasticity and incorporate more information from the past:

- Gradient. At every iteration, the gradient is estimated from a mini-batch. In order to bring MBF closer to a drop-in replacement for adaptive gradient methods such as Adam, we add momentum to the mini-batch gradient, let:

$$\widehat{\mathcal{D}\mathbf{W}_l} = \mu \widehat{\mathcal{D}\mathbf{W}_l} + \overline{\mathcal{D}\mathbf{W}_l}$$

We then apply the preconditioner to $\widehat{\mathcal{D}\mathbf{W}_l}$ to compute the update step.

- We also use a moving average scheme to get a better estimate of the Fisher mini-blocks, i.e.

$$\widehat{G_{\mathbf{W}_{l,b}}} = \beta \widehat{G_{\mathbf{W}_{l,b}}} + (1 - \beta) \overline{G_{\mathbf{W}_{l,b}}},$$

where $\overline{G_{\mathbf{W}_{l,b}}}$ is the current approximation to the mini-block Fisher matrix defined in the next paragraph.

Approximating the mini-block Fisher matrices: As mentioned previously, computing the matrices $\overline{G_{\mathbf{W}_{l,b}}} := \frac{1}{m} (\mathbf{J}^{\mathbf{W}_{l,b}})^T \mathbf{J}^{\mathbf{W}_{l,b}}$ to update the Fisher mini-blocks is inefficient in practice as this requires storing and computing the

Table 1: Storage Requirements

Algorithm	$\mathcal{D}W$	P_l
MBF	$O(IJ \Delta)$	$O(IJ \Delta ^2)$
KFAC	$O(IJ \Delta)$	$O(J^2 \Delta ^2 + I^2)$
Adam	$O(IJ \Delta)$	$O(IJ \Delta)$

Table 2: Computation per iteration beyond that required for the minibatch stochastic gradient

Algorithm	Additional pass	Curvature	Step ΔW_l
MBF	—	$O(\frac{IJ \Delta ^2}{T_1} + \frac{IJ \Delta ^3}{T_2})$	$O(IJ \Delta ^2)$
KFAC	$O(\frac{mIJ \Delta \mathcal{T} }{T_1})$	$O(\frac{m(J^2 \Delta ^2 + I^2) \mathcal{T} }{T_1} + \frac{J^3 \Delta ^3 + I^3}{T_2})$	$O(IJ^2 \Delta ^2 + I^2J \Delta)$
Adam	—	$O(IJ \Delta)$	$O(IJ \Delta)$

individual gradients, we propose approximating these mini-block matrices by the outer product of the part of the mini-batch gradient corresponding to the subset of weights $W_{l,b}$, i.e., $\bar{G}_{W_{l,b}} \approx (\bar{\mathcal{D}W}_{l,b})(\bar{\mathcal{D}W}_{l,b})^\top$.

Spatial average for large fully connected layers: In some CNN and auto-encoder models, using the Fisher mini-blocks can still be computationally prohibitive for ff-fc layers where both the input and output dimensions are large. Therefore, for such layers we used a Spatial Averaging technique, similar to one used in (Yao et al., 2021), where we used and maintained a single preconditioning matrix for all the mini-blocks by averaging the approximate mini-block Fisher matrices whenever we updated the preconditioning matrix. This technique also leads to more stable curvature updates as a side benefit, as observed for the method proposed in (Yao et al., 2021), where the Hessian diagonal was "smoothed" across each layer.

Amortized updates of the preconditioning matrices: The extra work for the above computations, as well as for updating the inverses $F_{W_{l,j}}^{-1}$ compared with first-order methods is amortized by only performing the Fisher matrix updates every T_1 iterations and computing their inverses every T_2 iterations. This approach which is also used in KFAC and Shampoo, does not seem to degrade MBF's overall performance, in terms of computational speed.

Comparison of Memory and Per-iteration Time Complexity. In Tables 1 and 2, we compare the space and computational requirements of the proposed MBF method with KFAC (see Appendix B.1) and Adam, which are among the predominant 2nd and 1st-order methods, respectively, used to train DNNs. We focus on one convolutional layer, with J input channels, I output channels, kernel size $|\Delta| = (2R + 1)^2$, and $|\mathcal{T}|$ spacial locations. Let m denote the size of the minibatches, and T_1 and T_2 denote, respectively, the frequency for updating the preconditioners and inverting them for both KFAC and MBF. From Table 1, we can see that MBF requires the same order of magnitude amount of memory as Adam (specifically, more by a factor of $|\Delta|$, which is usually small in most CNN architectures; e.g, in VGG16 (Simonyan & Zisserman, 2014) $|\Delta| = 9$). In Table 2, we also see that MBF requires only a small amount more per-iteration time than Adam (i.e., by a factor of $(\frac{|\Delta|}{T_1} + \frac{|\Delta|^2}{T_2} + |\Delta|)$). Note that in our experiments, $T_1 \approx |\Delta|$ and $T_2 \approx |\Delta|^2$.

Our MBF algorithm is described fully as Algorithm 2 below.

8. Experiments

In this section, we compare MBF with some SOTA first-order (SGD-m, Adam) and second-order (KFAC, Shampoo) methods. (See Appendix B.1 on how these methods were implemented.) Since MBF uses information about the second-moment of the gradient to construct a preconditioning matrix, Adam, KFAC and Shampoo were obvious choices for comparison with MBF.

Our experiments were run on a machine with one V100 GPU and eight Xeon Gold 6248 CPUs using PyTorch (Paszke et al., 2019). Each algorithm was run using the best hyper-parameters, determined by a grid search (specified in Appendices B.3 and B.2), and 5 different random seeds. The performance of MBF and the comparison algorithms is plotted in Figures 6 and 7: the solid curves depict the results averaged over the 5 different runs, and the shaded areas depict the \pm standard deviation range for these runs.

Algorithm 2 Mini-Block Fisher method (MBF)

Require: Given batch size m , learning rate $\{\eta_k\}_{k \geq 1}$, weight decay factor γ , damping value λ , statistics update frequency T_1 , inverse update frequency T_2

- 1: $\mu = 0.9, \beta = 0.9$
- 2: Initialize $\widehat{G}_{l,b} = \mathbb{E}[G_{l,b}]$ ($l = 1, \dots, k$, mini-blocks b) by iterating through the whole dataset, $\widehat{DW}_{l,b} = 0$ ($l = 1, \dots, k$, mini-blocks b)
- 3: **for** $k = 1, 2, \dots$ **do**
- 4: Sample mini-batch M_t of size m
- 5: Perform a forward-backward pass over M_t to compute the mini-batch gradient $\overline{DW}_{l,b}$
- 6: **for** $l = 1, \dots, L$ **do**
- 7: **for** mini-block b in layer l , **in parallel do**
- 8: $\widehat{DW}_{l,b} = \mu \overline{DW}_{l,b} + \overline{DW}_{l,b}$
- 9: **if** $k \equiv 0 \pmod{T_1}$ **then**
- 10: If Layer l is convolutional: $\widehat{G}_{l,j,i} = \beta \widehat{G}_{l,j,i} + (1 - \beta) \overline{DW}_{l,j,i} (\overline{DW}_{l,j,i})^\top$
- 11: If Layer l is fully-connected: $\widehat{G}_l = \beta \widehat{G}_l + \frac{1-\beta}{O} \sum_{j=1}^O \overline{DW}_{l,j} (\overline{DW}_{l,j})^\top$
- 12: **end if**
- 13: **if** $k \equiv 0 \pmod{T_2}$ **then**
- 14: Recompute and store $(\widehat{G}_{l,b} + \lambda I)^{-1}$
- 15: **end if**
- 16: $p_{l,b} = (\widehat{G}_{l,b} + \lambda I)^{-1} \widehat{DW}_{l,b} + \gamma W_{l,b}$
- 17: $W_{l,b} = W_{l,b} - \eta_k p_{l,b}$
- 18: **end for**
- 19: **end for**
- 20: **end for**

8.1. Generalization performance: CNNs

We first compared the generalization performance of MBF to SGD-m, Adam, KFAC and Shampoo on three CNN models, namely, ResNet32 (He et al., 2016), VGG16 (Simonyan & Zisserman, 2014) and VGG11 (Simonyan & Zisserman, 2014), respectively, on the datasets CIFAR-10, CIFAR-100 and SVHN (Krizhevsky et al., 2009). The first two have 50,000 training data and 10,000 testing data (used as the validation set in our experiments), while SVHN has 73,257 training data and 26,032 testing data. For all algorithms, we used a batch size of 128. In training, we applied data augmentation as described in (Krizhevsky et al., 2012), including random horizontal flip and random crop, since these setting choices have been used and endorsed in many previous research papers, e.g. Zhang et al. (2019b); Choi et al. (2019); Ren & Goldfarb (2021b). (see Appendix B for more details about the experimental set-up)

On all three model/dataset problems, the first-order methods were run for 200 epochs, and KFAC and Shampoo for 100 epochs, while MBF was run for 150 epochs on VGG16/CIFAR-100 and VGG11/SVHN, and 200 epochs on ResNet32/CIFAR-10. The reason that we ran MBF for 200 epochs (i.e., the same number as run for Adam) on ResNet32 was because all of ResNet32’s convolutional layers use small (3×3) kernels, and it contains just one fully connected layer of modest size (I, O) = (64, 10). Hence as we expected, MBF and Adam took almost the same time to complete 200 epochs. As can be seen in Figure 6, MBF could have been terminated after 150 epochs, without a significant change in validation error. On the other hand, since VGG16 and VGG11 have two large fully connected-layers (e.g [4096, 4096, 10/100]), MBF’s per-iteration computational cost is substantially larger than Adam’s due to these layers. Consequently, for both methods to finish roughly in the same amount of time, we ran MBF for only 150 epochs.

All methods employed a learning rate (LR) schedule that decayed LR by a factor of 0.1 every K epochs, where K was set to 40, 50 and 60, for the first-order methods, MBF, and KFAC/Shampoo, respectively, on the VGG16 and VGG11 problems, and set to 40, 60, and 80, respectively, on the ResNet32 problem

Moreover, weight decay, which has been shown to improve generalization across different optimizers (Loshchilov & Hutter, 2019; Zhang et al., 2019b), was employed by all of the algorithms, and a grid search on the weight decay factor and the initial learning rate based on the criteria of maximal validation classification accuracy, was performed. Finally, the damping parameter was set to $1e-8$ for Adam (following common practice), and 0.03 for KFAC (<https://github.com/zhaochen1992/kfac>).

([//github.com/alecwangcq/KFAC-Pytorch](https://github.com/alecwangcq/KFAC-Pytorch)). For Shampoo, we set $\epsilon = 0.01$. For MBF, we set $\lambda = 0.003$. We set $T_1 = 10$ and $T_2 = 100$ for KFAC, Shampoo and MBF.

From Figure 6, we see that MBF has a similar (and sometimes better) generalization performance than the other methods. Moreover, in terms of process time, MBF is roughly as fast as SGD-m and Adam on ResNet32/CIFAR-10 in Figure 6, and is competitive with all of the SOTA first and second-order methods in our experiments.

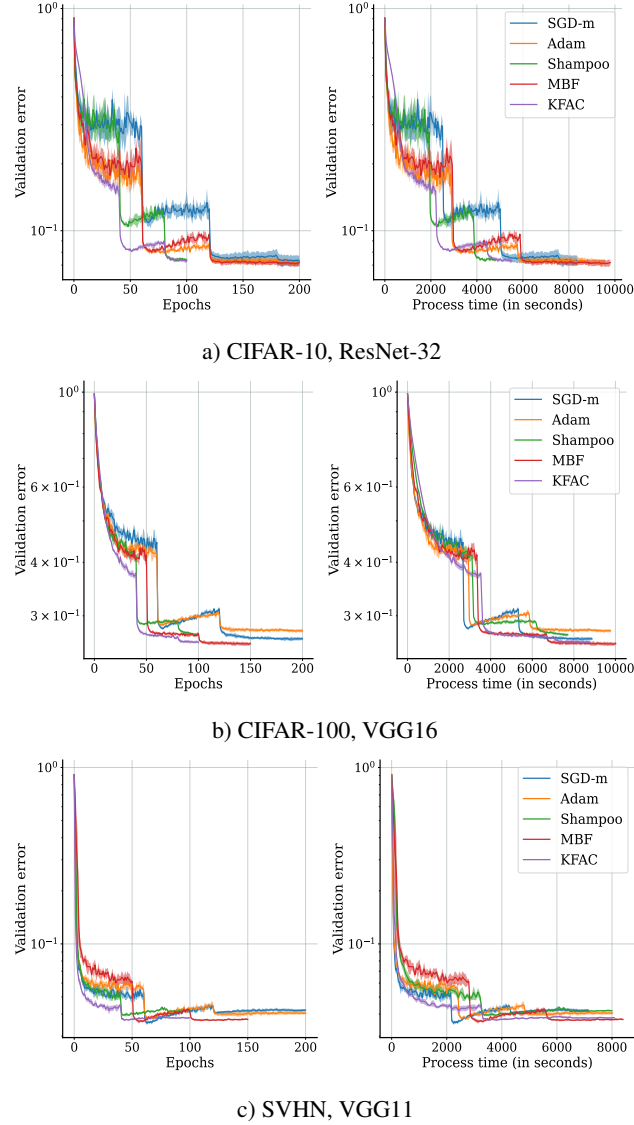


Figure 6: Generalization ability of MBF, KFAC, Shampoo, Adam, and SGD-m on three CNN problems.

8.2. Optimization performance: Autoencoder Problems

We also compared the optimization performance of the algorithms on three autoencoder problems (Hinton & Salakhutdinov, 2006) with datasets MNIST (LeCun et al., 2010), FACES², and CURVES³, which were also used for benchmarking algorithms in (Martens, 2010; Martens & Grosse, 2015; Botev et al., 2017; Goldfarb et al., 2020). The details of the layer shapes of the autoencoders are specified in Appendix B.2. For all algorithms, we used a batch size of 1,000, and settings that largely mimic the settings in the latter papers. Each algorithm was run for 500 seconds for MNIST and CURVES, and 2000

²<https://cs.nyu.edu/~roweis/data.html>

³Downloadable at www.cs.toronto.edu/~jmartens/digs3pts_1.mat

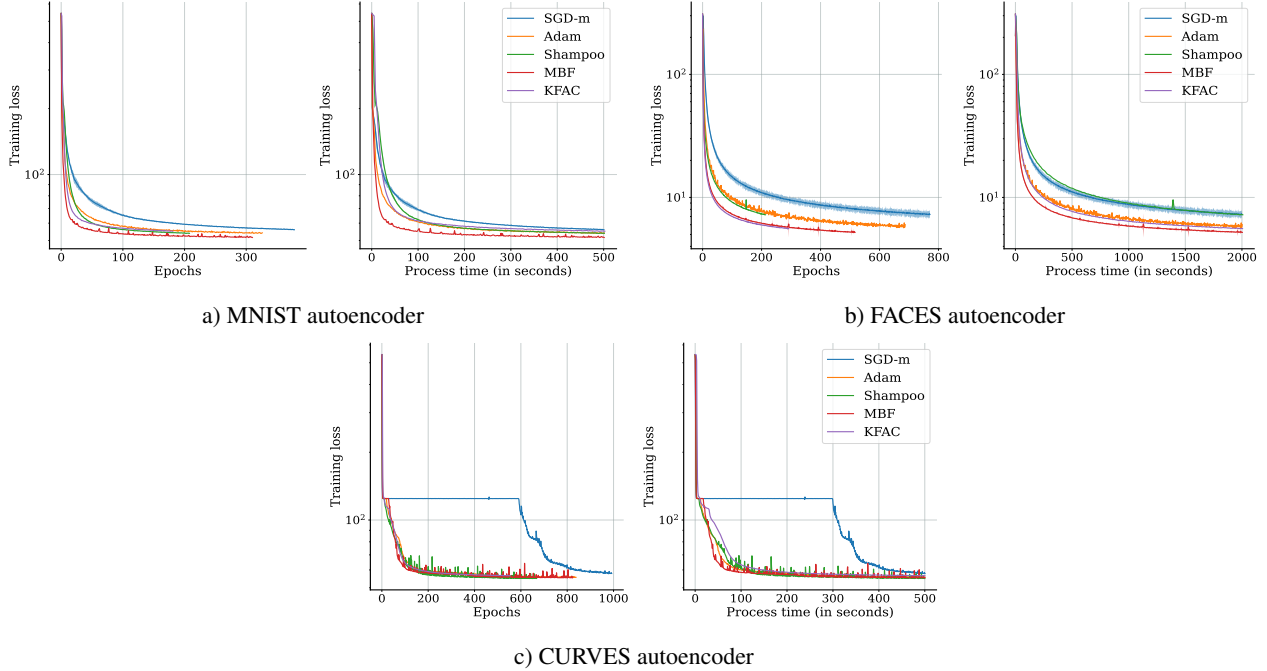


Figure 7: Optimization performance of MBF, KFAC, Shampoo, Adam, and SGD-m on three autoencoder problems

seconds for FACES.

For each algorithm, we conducted a grid search on the LR and damping value based on minimizing the training loss. We set the Fisher matrix update frequency $T_1 = 1$ and inverse update frequency $T_2 = 20$ for second-order methods, as in (Ren & Goldfarb, 2021b). From Figure 7, it is clear that MBF outperformed SGD-m and Adam, both in terms of per-epoch progress and process time. Moreover, MBF performed (at least) as well as KFAC and Shampoo. We postulate that the excellent performance of MBF is due to its ability to capture important curvature information from the mini-block Fisher matrix, while keeping the computational cost per iteration low and close to that of Adam.

9. Conclusion

We proposed a new approximate NG method, MBF, for training deep learning models. By approximating the Fisher matrix by a mini-block diagonal matrix that arises naturally from the structure of convolutional and ff-fc layers, MBF only requires very mild memory and computational overheads, compared with first-order methods. Moreover, it is easy to implement. Our experiments on various deep learning models and datasets, demonstrate conclusively that MBF provides comparable and sometimes better results than SOTA methods, both from an optimization and generalization perspective.

References

- Amari, S.-I., Park, H., and Fukumizu, K. Adaptive method of realizing natural gradient learning for multilayer perceptrons. *Neural computation*, 12(6):1399–1409, 2000.
- Anil, R., Gupta, V., Koren, T., Regan, K., and Singer, Y. Scalable second order optimization for deep learning. *arXiv preprint arXiv:2002.09018*, 2021.
- Botev, A., Ritter, H., and Barber, D. Practical gauss-newton optimisation for deep learning. In *International Conference on Machine Learning*, pp. 557–565. PMLR, 2017.
- Broyden, C. G. The convergence of a class of double-rank minimization algorithms 1. general considerations. *IMA Journal of Applied Mathematics*, 6(1):76–90, 1970.
- Byrd, R. H., Hansen, S. L., Nocedal, J., and Singer, Y. A stochastic quasi-newton method for large-scale optimization. *SIAM Journal on Optimization*, 26(2):1008–1031, 2016.
- Choi, D., Shallue, C. J., Nado, Z., Lee, J., Maddison, C. J., and Dahl, G. E. On empirical comparisons of optimizers for deep learning. *arXiv preprint arXiv:1910.05446*, 2019.
- Collobert, R. Large scale machine learning. Technical report, Université de Paris VI, 2004.
- Duchi, J., Hazan, E., and Singer, Y. Adaptive subgradient methods for online learning and stochastic optimization. *Journal of Machine Learning Research*, 12(Jul):2121–2159, 2011.
- Fletcher, R. A new approach to variable metric algorithms. *The computer journal*, 13(3):317–322, 1970.
- George, T., Laurent, C., Bouthillier, X., Ballas, N., and Vincent, P. Fast approximate natural gradient descent in a kronecker-factored eigenbasis. *arXiv preprint arXiv:1806.03884*, 2018.
- Goldfarb, D. A family of variable-metric methods derived by variational means. *Mathematics of computation*, 24(109): 23–26, 1970.
- Goldfarb, D., Ren, Y., and Bahamou, A. Practical quasi-newton methods for training deep neural networks. In Larochelle, H., Ranzato, M., Hadsell, R., Balcan, M. F., and Lin, H. (eds.), *Advances in Neural Information Processing Systems*, volume 33, pp. 2386–2396. Curran Associates, Inc., 2020.
- Gower, R., Goldfarb, D., and Richtárik, P. Stochastic block bfgs: Squeezing more curvature out of data. In *International Conference on Machine Learning*, pp. 1869–1878, 2016.
- Grosse, R. and Martens, J. A kronecker-factored approximate fisher matrix for convolution layers. In *International Conference on Machine Learning*, pp. 573–582. PMLR, 2016.
- Gupta, V., Koren, T., and Singer, Y. Shampoo: Preconditioned stochastic tensor optimization. In Dy, J. and Krause, A. (eds.), *Proceedings of the 35th International Conference on Machine Learning*, volume 80 of *Proceedings of Machine Learning Research*, pp. 1842–1850. PMLR, 2018.
- He, K., Zhang, X., Ren, S., and Sun, J. Deep residual learning for image recognition. In *Proceedings of the IEEE conference on computer vision and pattern recognition*, pp. 770–778, 2016.
- Heskes, T. On ”natural” learning and pruning in multilayered perceptrons. *Neural Computation*, 12, 01 2000. doi: 10.1162/089976600300015637.
- Hinton, G., Srivastava, N., and Swersky, K. Neural networks for machine learning lecture 6a overview of mini-batch gradient descent. *Cited on*, 14(8), 2012.
- Hinton, G. E. and Salakhutdinov, R. R. Reducing the dimensionality of data with neural networks. *science*, 313(5786): 504–507, 2006.
- Kingma, D. and Ba, J. Adam: A method for stochastic optimization. *International Conference on Learning Representations*, 2014.

- Krizhevsky, A., Hinton, G., et al. Learning multiple layers of features from tiny images. 2009.
- Krizhevsky, A., Sutskever, I., and Hinton, G. E. Imagenet classification with deep convolutional neural networks. *Advances in neural information processing systems*, 25:1097–1105, 2012.
- LeCun, Y., Cortes, C., and Burges, C. MNIST handwritten digit database. *ATT Labs [Online]*. Available: <http://yann.lecun.com/exdb/mnist>, 2, 2010.
- Liu, D. C. and Nocedal, J. On the limited memory bfgs method for large scale optimization. *Mathematical programming*, 45(1-3):503–528, 1989.
- Loshchilov, I. and Hutter, F. Decoupled weight decay regularization. In *International Conference on Learning Representations*, 2019.
- Martens, J. Deep learning via hessian-free optimization. In *ICML*, volume 27, pp. 735–742, 2010.
- Martens, J. New insights and perspectives on the natural gradient method. *Journal of Machine Learning Research*, 21(146): 1–76, 2020.
- Martens, J. and Grosse, R. Optimizing neural networks with kronecker-factored approximate curvature. In *International conference on machine learning*, pp. 2408–2417. PMLR, 2015.
- Nesterov, Y. Introductory lectures on convex programming volume i: Basic course. *Lecture notes*, 3(4):5, 1998.
- Ortega, J. and Rheinboldt, W. *Iterative Solution of Nonlinear Equations in Several Variables*. Classics in Applied Mathematics. Society for Industrial and Applied Mathematics (SIAM, 3600 Market Street, Floor 6, Philadelphia, PA 19104), 1970. ISBN 9780898719468.
- Paszke, A., Gross, S., Massa, F., Lerer, A., Bradbury, J., Chanan, G., Killeen, T., Lin, Z., Gimelshein, N., Antiga, L., Desmaison, A., Kopf, A., Yang, E., DeVito, Z., Raison, M., Tejani, A., Chilamkurthy, S., Steiner, B., Fang, L., Bai, J., and Chintala, S. Pytorch: An imperative style, high-performance deep learning library. In Wallach, H., Larochelle, H., Beygelzimer, A., d'Alché-Buc, F., Fox, E., and Garnett, R. (eds.), *Advances in Neural Information Processing Systems 32*, pp. 8024–8035. Curran Associates, Inc., 2019.
- Polyak, B. Some methods of speeding up the convergence of iteration methods. *Ussr Computational Mathematics and Mathematical Physics*, 4:1–17, 12 1964. doi: 10.1016/0041-5553(64)90137-5.
- Povey, D., Zhang, X., and Khudanpur, S. Parallel training of dnns with natural gradient and parameter averaging. *arXiv preprint arXiv:1410.7455*, 2014.
- Ren, Y. and Goldfarb, D. Efficient subsampled gauss-newton and natural gradient methods for training neural networks. *arXiv preprint arXiv:1906.02353*, 2019.
- Ren, Y. and Goldfarb, D. Kronecker-factored quasi-Newton methods for convolutional neural networks. *arXiv preprint arXiv:2102.06737*, 2021a.
- Ren, Y. and Goldfarb, D. Tensor normal training for deep learning models. *arXiv preprint arXiv:2106.02925*, 2021b.
- Robbins, H. and Monro, S. A stochastic approximation method. *The annals of mathematical statistics*, pp. 400–407, 1951.
- Roux, N., Manzagol, P.-a., and Bengio, Y. Topmoumoute online natural gradient algorithm. In Platt, J., Koller, D., Singer, Y., and Roweis, S. (eds.), *Advances in Neural Information Processing Systems*, volume 20. Curran Associates, Inc., 2008.
- Schmidt, R. M., Schneider, F., and Hennig, P. Descending through a crowded valley - benchmarking deep learning optimizers, 2021.
- Shallue, C. J., Lee, J., Antognini, J., Sohl-Dickstein, J., Frostig, R., and Dahl, G. E. Measuring the effects of data parallelism on neural network training, 2019.
- Shanno, D. F. Conditioning of quasi-newton methods for function minimization. *Mathematics of computation*, 24(111): 647–656, 1970.

- Simonyan, K. and Zisserman, A. Very deep convolutional networks for large-scale image recognition. *arXiv preprint arXiv:1409.1556*, 2014.
- Soori, S., Can, B., Mu, B., Gürbüzbalaban, M., and Dehnavi, M. M. Tengerad: Time-efficient natural gradient descent with exact fisher-block inversion. *CoRR*, abs/2106.03947, 2021.
- Vinyals, O. and Povey, D. Krylov subspace descent for deep learning. In *Artificial Intelligence and Statistics*, pp. 1261–1268, 2012.
- Wang, M., Fang, E. X., and Liu, B. Stochastic compositional gradient descent: Algorithms for minimizing compositions of expected-value functions. *Mathematical Programming*, 161(1-2):419–449, 2017.
- Xiao, H., Rasul, K., and Vollgraf, R. Fashion-mnist: a novel image dataset for benchmarking machine learning algorithms. *arXiv preprint arXiv:1708.07747*, 2017.
- Xu, P., Roosta, F., and Mahoney, M. W. Newton-type methods for non-convex optimization under inexact hessian information. *Mathematical Programming*, pp. 1–36, 2019.
- Yao, Z., Gholami, A., Shen, S., Keutzer, K., and Mahoney, M. W. Adahessian: An adaptive second order optimizer for machine learning. *AAAI (Accepted)*, 2021.
- Zhang, G., Martens, J., and Grosse, R. Fast convergence of natural gradient descent for overparameterized neural networks. *arXiv preprint arXiv:1905.10961*, 2019a.
- Zhang, G., Wang, C., Xu, B., and Grosse, R. Three mechanisms of weight decay regularization. In *International Conference on Learning Representations*, 2019b.

A. Proof of Convergence of Algorithm MBF and Associated Lemmas

We follow the framework used in (Zhang et al., 2019a) to prove linear convergence of NG descent, to provide similar convergence guarantees for our idealized MBF Algorithm, with exact gradients (i.e. full batch case with $m = n$)⁴.

Proof of Theorem 1. If Assumption 6.2 holds, then one can obtain a lower bound on the minimum eigenvalue of the mini-block Fisher matrix $F_{MB}(\mathbf{W}(k)) = \frac{1}{n} \mathbf{J}_{MB}(k)^\top \mathbf{J}_{MB}(k)$ at each iteration.

In fact, if $\|\mathbf{W}(k) - \mathbf{W}(0)\|_2 \leq \frac{3}{\sqrt{\lambda_0}} \|\mathbf{y} - \mathbf{u}(0)\|_2$, then, by Assumption 6.2, there exists $0 < C \leq \frac{1}{2}$ that satisfies $\|\mathbf{J}(\mathbf{W}(k)) - \mathbf{J}(\mathbf{W}(0))\|_2 \leq \frac{C}{3} \sqrt{\lambda_0}$, and therefore, we have that

$$\|\mathbf{J}_{MB}(k) - \mathbf{J}_{MB}(0)\|_2 \leq \frac{C\sqrt{\lambda_0}}{3} \leq \frac{\sqrt{\lambda_0}}{3}.$$

On the other hand, based on the inequality $\sigma_{\min}(\mathbf{A} + \mathbf{B}) \geq \sigma_{\min}(\mathbf{A}) - \sigma_{\max}(\mathbf{B})$, where σ denotes singular value, we have

$$\begin{aligned} \sigma_{\min}(\mathbf{J}_{MB}(k)) &\geq \sigma_{\min}(\mathbf{J}_{MB}(0)) - \sigma_{\min}(\mathbf{J}_{MB}(k) - \mathbf{J}_{MB}(0)) \\ &\geq \sigma_{\min}(\mathbf{J}_{MB}(0)) - \|\mathbf{J}_{MB}(k) - \mathbf{J}_{MB}(0)\|_2 \geq \sqrt{\lambda_0} - \frac{\sqrt{\lambda_0}}{3} = \frac{2\sqrt{\lambda_0}}{3}. \end{aligned}$$

Therefore

$$\lambda_{\min}(\mathbf{G}_{MB}(\mathbf{W}(k))) \geq \frac{4\sqrt{\lambda_0}}{9}.$$

where $\mathbf{G}_{MB}(\mathbf{W}(k)) := \mathbf{J}_{MB}(\mathbf{W}(k)) \mathbf{J}_{MB}(\mathbf{W}(k))^\top$ is the mini-block Gram matrix. We prove Theorem 1 by induction. Assume $\|\mathbf{u}(\mathbf{W}(k)) - \mathbf{y}\|_2^2 \leq (1 - \eta)^k \|\mathbf{u}(\mathbf{W}(0)) - \mathbf{y}\|_2^2$. One can see that the relationship between the Jacobian $\mathbf{J}(\mathbf{W}(k))$ and the mini-Block Jacobian $\mathbf{J}_{MB}(\mathbf{W}(k))$ is:

$$\mathbf{J}^\top(\mathbf{W}(k)) = \mathbf{J}_{MB}(\mathbf{W}(k))^\top \mathbf{K},$$

where the matrix $\mathbf{K} = \underbrace{[I_n, \dots, I_n]^\top}_{\mathbf{K}} \in \mathbb{R}^{Kn \times n}$, I_n is the identity matrix of dimension n , the number of samples, and K is the total number of mini-blocks. We define

$$\mathbf{W}_k(s) = s\mathbf{W}(k+1) + (1-s)\mathbf{W}(k) = \mathbf{W}(k) - s \frac{\eta}{n} (\mathbf{F}_{MB}(\mathbf{W}(k)) + \lambda I)^{-1} \mathbf{J}(\mathbf{W}(k))^\top (\mathbf{u}(\mathbf{W}(k)) - \mathbf{y}) - \mathbf{u}(\mathbf{W}(k)),$$

we have:

$$\begin{aligned} \mathbf{u}(\mathbf{W}(k+1)) - \mathbf{u}(\mathbf{W}(k)) &= \mathbf{u}(\mathbf{W}(k) - \frac{\eta}{n} (\mathbf{F}_{MB}(\mathbf{W}(k)) + \lambda I)^{-1} \mathbf{J}(\mathbf{W}(k))^\top (\mathbf{u}(\mathbf{W}(k)) - \mathbf{y})) - \mathbf{u}(\mathbf{W}(k)) \\ &= - \int_{s=0}^1 \left\langle \frac{\partial \mathbf{u}(\mathbf{W}_k(s))}{\partial \mathbf{W}^\top}, \frac{\eta}{n} (\mathbf{F}_{MB}(\mathbf{W}(k)) + \lambda I)^{-1} \mathbf{J}(\mathbf{W}(k))^\top (\mathbf{u}(\mathbf{W}(k)) - \mathbf{y}) \right\rangle ds \\ &= - \underbrace{\int_{s=0}^1 \left\langle \frac{\partial \mathbf{u}(\mathbf{W}(k))}{\partial \mathbf{W}^\top}, \frac{\eta}{n} (\mathbf{F}_{MB}(\mathbf{W}(k)) + \lambda I)^{-1} \mathbf{J}(\mathbf{W}(k))^\top (\mathbf{u}(\mathbf{W}(k)) - \mathbf{y}) \right\rangle ds}_{\text{(A)}} \\ &\quad + \underbrace{\int_{s=0}^1 \left\langle \frac{\partial \mathbf{u}(\mathbf{W}(k))}{\partial \mathbf{W}^\top} - \frac{\partial \mathbf{u}(\mathbf{W}_k(s))}{\partial \mathbf{W}^\top}, \frac{\eta}{n} (\mathbf{F}_{MB}(\mathbf{W}(k)) + \lambda I)^{-1} \mathbf{J}(\mathbf{W}(k))^\top (\mathbf{u}(\mathbf{W}(k)) - \mathbf{y}) \right\rangle ds}_{\text{(B)}} \end{aligned}$$

In what follows, to simplify the notation, we drop $\mathbf{W}(k)$ whenever the context is clear. Thus, we have

$$\text{(A)} = \frac{\eta}{n} \mathbf{J} (\mathbf{F}_{MB} + \lambda I)^{-1} \mathbf{J}^\top (\mathbf{y} - \mathbf{u}(k)). \quad (3)$$

⁴in (Soori et al., 2021), a similar extension of the proof in (Zhang et al., 2019a) is used to analyse the convergence of a layer-wise block Fisher method.

Now, we bound the norm of $\textcircled{\mathbf{B}}$:

$$\begin{aligned}
 \|\textcircled{\mathbf{B}}\|_2 &\leq \frac{\eta}{n} \left\| \int_{s=0}^1 \mathbf{J}(\mathbf{W}_k(s)) - \mathbf{J}(\mathbf{W}(k)) ds \right\|_2 \left\| (\mathbf{F}_{MB} + \lambda I)^{-1} \mathbf{J}^\top(\mathbf{u}(k) - \mathbf{y}) \right\|_2 \\
 &\stackrel{(1)}{\leq} \frac{\eta 2C}{3n} \lambda_0^{\frac{1}{2}} \left\| \left(\frac{1}{n} \mathbf{J}_{MB}^\top \mathbf{F}_{MB} + \lambda I \right)^{-1} \mathbf{F}_{MB}^\top \mathbf{K}(\mathbf{u}(k) - \mathbf{y}) \right\|_2 \\
 &\leq \frac{\eta 2C}{3n} \lambda_0^{\frac{1}{2}} \left\| \left(\frac{1}{n} \mathbf{J}_{MB}^\top \mathbf{J}_{MB} + \lambda I \right)^{-1} \mathbf{J}_{MB}^\top \right\|_2 \|\mathbf{K}(\mathbf{u}(k) - \mathbf{y})\|_2 \\
 &\stackrel{(2)}{\leq} \frac{\eta C}{3\sqrt{\lambda n}} \sqrt{\lambda_0} \|\mathbf{K}(\mathbf{u}(k) - \mathbf{y})\|_2 \stackrel{(3)}{=} \frac{\eta C \sqrt{\lambda_0 K}}{3\sqrt{\lambda n}} \|(\mathbf{u}(k) - \mathbf{y})\|_2,
 \end{aligned} \tag{4}$$

where in (1) we used Assumption 6.2, which implies

$$\begin{aligned}
 \left\| \int_{s=0}^1 \mathbf{J}(\mathbf{W}_k(s)) - \mathbf{J}(\mathbf{W}(k)) ds \right\|_2 &\leq \|\mathbf{J}(\mathbf{W}(k)) - \mathbf{J}(\mathbf{W}(0))\|_2 + \|\mathbf{J}(\mathbf{W}(k+1)) - \mathbf{J}(\mathbf{W}(0))\|_2 \\
 &\leq \frac{2C}{3} \sqrt{\lambda_0}.
 \end{aligned}$$

The inequality (2) follows from the fact that

$$\begin{aligned}
 \left\| \left(\frac{1}{n} \mathbf{J}_{MB}^\top \mathbf{J}_{MB} + \lambda I \right)^{-1} \mathbf{J}_{MB}^\top \right\|_2 &= \sigma_{\max} \left(\left(\frac{1}{n} \mathbf{J}_{MB}^\top \mathbf{J}_{MB} + \lambda I \right)^{-1} \mathbf{J}_{MB}^\top \right) \\
 &= \sqrt{\lambda_{\max} \left(\mathbf{J}_{MB} \left(\frac{1}{n} \mathbf{J}_{MB}^\top \mathbf{J}_{MB} + \lambda I \right)^{-2} \mathbf{J}_{MB}^\top \right)},
 \end{aligned}$$

and that

$$\lambda_{\max} \left(\mathbf{J}_{MB} \left(\frac{1}{n} \mathbf{J}_{MB}^\top \mathbf{J}_{MB} + \lambda I \right)^{-2} \mathbf{J}_{MB}^\top \right) = \max_{\mu \text{ eigenvalue of } \mathbf{G}_{MB}} \frac{\mu}{\left(\frac{\mu}{n} + \lambda \right)^2} \leq \frac{n\lambda}{\left(\frac{n\lambda}{n} + \lambda \right)^2} = \frac{n}{4\lambda}.$$

and in the equality (3), we have used the fact that $\|\mathbf{K}(\mathbf{u}(k) - \mathbf{y})\|_2 = \sqrt{K} \|(\mathbf{u}(k) - \mathbf{y})\|_2$. Finally, we have:

$$\begin{aligned}
 \|\mathbf{u}(k+1) - \mathbf{y}\|_2^2 &= \|\mathbf{u}(k) - \mathbf{y} + \mathbf{u}(k+1) - \mathbf{u}(k)\|_2^2 \\
 &= \|\mathbf{u}(k) - \mathbf{y}\|_2^2 - 2(\mathbf{y} - \mathbf{u}(k))^\top (\mathbf{u}(k+1) - \mathbf{u}(k)) + \|\mathbf{u}(k+1) - \mathbf{u}(k)\|_2^2 \\
 &\leq \|\mathbf{u}(k) - \mathbf{y}\|_2^2 - \frac{2\eta}{n} \underbrace{(\mathbf{y} - \mathbf{u}(k))^\top \mathbf{J}(k) (\mathbf{F}_{MB} + \lambda I)^{-1} \mathbf{J}(k)^\top (\mathbf{y} - \mathbf{u}(k))}_{\textcircled{1}} \\
 &\quad + \frac{2\eta C \sqrt{\lambda_0 K}}{3\sqrt{\lambda n}} \|\mathbf{u}(k) - \mathbf{y}\|_2^2 + \underbrace{\|\mathbf{u}(k+1) - \mathbf{u}(k)\|_2^2}_{\textcircled{2}} \\
 &\leq \|\mathbf{u}(k) - \mathbf{y}\|_2^2 - \frac{2\eta K \lambda_0}{\lambda_0 + \frac{9}{4}n\lambda} \|\mathbf{u}(k) - \mathbf{y}\|_2^2 + \frac{2\eta C \sqrt{\lambda_0 K}}{3\sqrt{\lambda n}} \|\mathbf{u}(k) - \mathbf{y}\|_2^2 + \eta^2 \left(K + \frac{C \sqrt{\lambda_0 K}}{3\sqrt{\lambda n}} \right)^2 \|\mathbf{u}(k) - \mathbf{y}\|_2^2 \\
 &\leq (1 - \eta) \|\mathbf{u}(k) - \mathbf{y}\|_2^2 \\
 &\quad + \eta \|\mathbf{u}(k) - \mathbf{y}\|_2^2 \left(\eta \left(K + \frac{C \sqrt{\lambda_0 K}}{3\sqrt{\lambda n}} \right)^2 - \left(\frac{2K \lambda_0}{\lambda_0 + \frac{9}{4}n\lambda} - \frac{2C \sqrt{\lambda_0 K}}{3\sqrt{\lambda n}} - 1 \right) \right).
 \end{aligned}$$

Part ① is lower bounded as follows:

$$\begin{aligned}
 \textcircled{1} &\geq \lambda_{\min} \left(\mathbf{J}_{MB} \left(\frac{1}{n} \mathbf{J}_{MB}^\top \mathbf{J}_{MB} + \lambda I \right)^{-1} \mathbf{J}_{MB}^\top \right) \|\mathbf{K}(\mathbf{u}(k) - \mathbf{y})\|_2^2 \\
 &= K \lambda_{\min} \left(\mathbf{J}_{MB} \left(\frac{1}{n} \mathbf{J}_{MB}^\top \mathbf{J}_{MB} + \lambda I \right)^{-1} \mathbf{J}_{MB}^\top \right) \|\mathbf{u}(k) - \mathbf{y}\|_2^2 = nK \|\mathbf{u}(k) - \mathbf{y}\|_2^2 \frac{\lambda_{\min}(\mathbf{G}_{MB}(k))}{\lambda_{\min}(\mathbf{G}_{MB}(k)) + n\lambda} \\
 &\geq \frac{nK\lambda_0}{\lambda_0 + \frac{9}{4}n\lambda} \|\mathbf{u}(k) - \mathbf{y}\|_2^2.
 \end{aligned}$$

Part ② is upper bounded, on the other hand, using equality (3) and inequality (4). More specifically, we have:

$$\begin{aligned}
 \|\mathbf{u}(k+1) - \mathbf{u}(k)\|_2 &\leq \frac{\eta}{n} \left\| \mathbf{J}(k) (\mathbf{F}_{MB} + \lambda I)^{-1} \mathbf{J}(k)^\top (\mathbf{y} - \mathbf{u}(k)) \right\| + \|\textcircled{\mathbf{B}}\|_2 \\
 &\leq \frac{\eta K}{n} \left\| \mathbf{J}_{MB}(k) (\mathbf{F}_{MB} + \lambda I)^{-1} \mathbf{J}_{MB}(k)^\top \right\| \|\mathbf{u}(k) - \mathbf{y}\|_2 + \frac{\eta C \sqrt{\lambda_0 K}}{3\sqrt{\lambda n}} \|\mathbf{u}(k) - \mathbf{y}\|_2 \\
 &\leq \eta \left(K + \frac{C \sqrt{\lambda_0 K}}{3\sqrt{\lambda n}} \right) \|\mathbf{u}(k) - \mathbf{y}\|_2.
 \end{aligned}$$

The last inequality follows from the fact that if (μ, v) is an (eigenvalue, eigenvector) pair for $\mathbf{G}_{MB} = \mathbf{J}_{MB} \mathbf{J}_{MB}^\top$, then $(\mu, \mathbf{J}_{MB}^\top v)$ and $(\frac{1}{\mu + \lambda}, \mathbf{J}_{MB}^\top v)$ are such pairs for \mathbf{F}_{MB} and $(\frac{1}{n} \mathbf{F}_{MB} + \lambda I)^{-1}$, respectively, and it follows that

$$\begin{aligned}
 \left\| \mathbf{J}_{MB}(k) (\mathbf{F}_{MB} + \lambda I)^{-1} \mathbf{J}_{MB}(k)^\top \right\|_2 &= \lambda_{\max} \left(\mathbf{J}_{MB}(k) (\mathbf{F}_{MB} + \lambda I)^{-1} \mathbf{J}_{MB}(k)^\top \right) \\
 &= \max_{\mu \text{ eigenvalue of } \mathbf{G}_{MB}(k)} \frac{n\mu}{\mu + n\lambda} \leq n.
 \end{aligned}$$

Let us consider the function $\lambda \xrightarrow{f} f(\lambda) := \left(\frac{2K\lambda_0}{\lambda_0 + \frac{9}{4}n\lambda} - \frac{2C\sqrt{\lambda_0 K}}{3\sqrt{\lambda n}} - 1 \right)$. We have that

$$f\left(\frac{4\lambda_0}{9n}\right) = K - C\sqrt{K} - 1 \geq K - \frac{1}{2}\sqrt{K} - 1 > 0 \quad \text{for } K \geq 3.$$

Therefore by continuity of the function $f(\cdot)$, there exists an interval $[\underline{\lambda}, \bar{\lambda}]$, such as $\frac{4\lambda_0}{9n} \in [\underline{\lambda}, \bar{\lambda}]$, and for all damping values λ in $[\underline{\lambda}, \bar{\lambda}]$, the function $f(\cdot)$ is positive. For such choice of damping value λ (for example $\lambda = \frac{4\lambda_0}{9n}$), and for a small enough learning rate, i.e:

$$\eta \leq \frac{\frac{2K\lambda_0}{\lambda_0 + \frac{9}{4}n\lambda} - \frac{2C\sqrt{\lambda_0 K}}{3\sqrt{\lambda n}} - 1}{\left(K + \frac{C\sqrt{\lambda_0 K}}{3\sqrt{\lambda n}} \right)^2} := \eta_\lambda.$$

We Hence, we get that

$$\|\mathbf{u}(k+1) - \mathbf{y}\|_2^2 \leq (1 - \eta) \|\mathbf{u}(k) - \mathbf{y}\|_2^2,$$

which concludes the proof.

B. Experiment Details

B.1. Competing Algorithms

B.1.1. SGD-M

In SGD with momentum, we updated the momentum m_t of the gradient using the recurrence

$$m_t = \mu \cdot m_{t-1} + g_t$$

at every iteration, where g_t denotes the mini-batch gradient at current iteration and $\mu = 0.9$. The gradient momentum is also used in the second-order methods, in our implementations. For the CNN problems, we used weight decay with SGD-m, similarly to how it is used in SGDW in (Loshchilov & Hutter, 2019). (For further details, see Section ??).

B.1.2. ADAM

For Adam, we followed exactly the algorithm in (Kingma & Ba, 2014) with $\beta_1 = 0.9$ and $\beta_2 = 0.999$, updating the momentum of gradient at every iteration by the recurrence

$$m_t = \beta_1 \cdot m_t - 1 + (1 - \beta_1) \cdot g_t.$$

The role of β_1 and β_2 is similar to that of μ and β in Algorithms 2 and 3, as we will describe below. For the CNN problems, we used weight decay Adam, similarly to how it is used in AdamW in (Loshchilov & Hutter, 2019).

B.1.3. SHAMPOO

We implemented Shampoo as described below in Algorithm 3 following the description given in (Gupta et al., 2018), and includes major improvements, following the suggestions in (Anil et al., 2021). These improvements are (i) using a moving average to update the estimates $\widehat{G}_l^{(i)}$ and (ii) using a coupled Newton method to compute inverse roots of the preconditioning matrices,

Algorithm 3 Shampoo

Require: Given batch size m , learning rate $\{\eta_k\}_{k \geq 1}$, weight decay factor γ , damping value ϵ , statistics update frequency T_1 , inverse update frequency T_2

- 1: $\mu = 0.9, \beta = 0.9$
- 2: Initialize $\widehat{G}_l^{(i)} = \mathbb{E}[G_l^{(i)}]$ ($l = 1, \dots, k, i = 1, \dots, k_l$) by iterating through the whole dataset, $\widehat{\nabla_{W_l} \mathcal{L}} = 0$ ($l = 1, \dots, L$)
- 3: **for** $k = 1, 2, \dots$ **do**
- 4: Sample mini-batch M_k of size m
- 5: Perform a forward-backward pass over the current mini-batch M_k to compute the minibatch gradient $\overline{\nabla \mathcal{L}}$
- 6: **for** $l = 1, \dots, L$ **do**
- 7: $\widehat{\nabla_{W_l} \mathcal{L}} = \mu \widehat{\nabla_{W_l} \mathcal{L}} + \overline{\nabla_{W_l} \mathcal{L}}$
- 8: **if** $k \equiv 0 \pmod{T_1}$ **then**
- 9: Update $\widehat{G}_l^{(i)} = \beta \widehat{G}_l^{(i)} + (1 - \beta) \overline{G}_l^{(i)}$ for $i = 1, \dots, k_l$ where $\overline{G}_l = \overline{\nabla_{W_l} \mathcal{L}}$
- 10: **end if**
- 11: **if** $k \equiv 0 \pmod{T_2}$ **then**
- 12: Recompute $\left(\widehat{G}_l^{(1)} + \epsilon I\right)^{-1/2k_l}, \dots, \left(\widehat{G}_l^{(k_l)} + \epsilon I\right)^{-1/2k_l}$ with the coupled Newton method
- 13: **end if**
- 14: $p_l = \widehat{\nabla_{W_l} \mathcal{L}} \times_1 \left(\widehat{G}_l^{(1)} + \epsilon I\right)^{-1/2k_l} \times_2 \dots \times_k \left(\widehat{G}_l^{(k_l)} + \epsilon I\right)^{-1/2k_l}$
- 15: $p_l = p_l + \gamma W_l$
- 16: $W_l = W_l - \eta_k \cdot p_l$
- 17: **end for**
- 18: **end for**

B.1.4. KFAC

In our implementation of KFAC, the preconditioning matrices that we used for linear layers and convolutional layers are precisely as those described in (Martens & Grosse, 2015) and (Grosse & Martens, 2016), respectively. For the parameters in the BN layers, we used the gradient direction, exactly as in <https://github.com/alecwangcq/KFAC-Pytorch>. We did a warm start to estimate the pre-conditioning KFAC matrices in an initialization step that iterated through the whole data set, and adopted a moving average scheme to update them with $\beta = 0.9$ afterwards. Similarly to the implementation described in (Ren & Goldfarb, 2021a), for autoencoder experiments, we inverted the damped KFAC matrices and used

Table 3: Storage Requirements for fully connected layer

Algorithm	\mathcal{DW}	P_l
MBF	$O(d_i d_o)$	$O(d_i^2)$
KFAC	$O(d_i d_o)$	$O(O(d_i^2 + d_o^2 + d_i d_o))$
Adam	$O(d_i d_o)$	$O(d_i d_o)$

Table 4: Computation per iteration beyond that required for the minibatch stochastic gradient for fully connected layer

Algorithm	Additional pass	Curvature	Step ΔW_l
MBF	—	$O(\frac{d_o d_i^2}{T_1} + \frac{d_i^3}{T_2})$	$O(d_o d_i^2)$
KFAC	$O(\frac{m d_i d_o}{T_1})$	$O(\frac{m d_i^2 + m d_o^2}{T_1} + \frac{d_i^3 + d_o^3}{T_2})$	$O(d_i^2 d_o + d_o^2 d_i)$
Adam	—	$O(d_i d_o)$	$O(d_i d_o)$

them to compute the updating direction, where the damping factors for both A and G were set to be $\sqrt{\lambda}$, where λ is the overall damping value; and for the CNN experiments, we followed the SVD (i.e. eigenvalue decomposition) implementation suggested in <https://github.com/alecwangcq/KFAC-Pytorch>, which, as we verified, performs better than splitting the damping value and inverting the damped KFAC matrices (as suggested in (Martens & Grosse, 2015; Grosse & Martens, 2016)). Further, for the CNN problems, we implemented weight decay exactly as in MBF (Algorithm 2) and Shampoo (Algorithm 3).

B.1.5. MBF-OTHER DETAILS

For the parameters in the BN layers, we used the direction used in Adam, which is equivalent to using mini-blocks of size 1, dividing each stochastic gradient component by that blocks square root. We did a warm start to estimate the pre-conditioning mini-block matrices in an initialization step that iterated through the whole data set, and adopted a moving average scheme to update them with $\beta = 0.9$ afterwards as described in Algorithm 2).

In Tables 3 and 4, we compared the space and computational requirements of the proposed MBF method with KFAC and Adam for a fully connected layer, with d_i inputs and d_o outputs. Note that these tables are the fully-connected analogs to Tables 1 and 2 in Section 7, which compare the storage and computational requirements for MBF, KFAC and Adam for a convolutional layer. Here, m denotes the size of the minibatches, and T_1 and T_2 denote, respectively, the frequency for updating the preconditioners and inverting them for both KFAC and MBF.

B.2. Experiment Settings for the Autoencoder Problems

Table 7 describes the model architectures of the autoencoder problems. The activation functions of the hidden layers are always ReLU, except that there is no activation for the very middle layer.

Table 5: DNN architectures for the MLP autoencoder problems

	Layer width
MNIST	[784, 1000, 500, 250, 30, 250, 500, 1000, 784]
FACES	[625, 2000, 1000, 500, 30, 500, 1000, 2000, 625]
CURVES	[784, 400, 200, 100, 50, 25, 6, 25, 50, 100, 200, 400, 784]

MNIST⁵, FACES⁶, and CURVES⁷ contain 60,000, 103,500, and 20,000 training samples, respectively, which we used in

⁵<http://yann.lecun.com/exdb/mnist/>

⁶http://www.cs.toronto.edu/~jmartens/newfaces_rot_single.mat

⁷http://www.cs.toronto.edu/~jmartens/digs3pts_1.mat

Table 6: Grid of hyper-parameters for autoencoder problems

Algorithm	learning rate	damping λ
SGD-m	1e-4, 3e-4, 0.001, 0.003, 0.01, 0.03	damping: not applicable
Adam	1e-5, 3e-5, 1e-4, 3e-4, 0.001, 0.003, 0.01	1e-8, 1e-4, 1e-2
Shampoo	1e-5, 3e-5, 1e-4, 3e-4, 0.001, 0.003	1e-4, 3e-4, 0.001, 0.003, 0.01
MBF	1e-7, 3e-7, 1e-6, 3e-6, 1e-5, 3e-5, 1e-4	1e-5, 3e-5, 1e-4, 3e-4, 0.001, 0.003, 0.01
KFAC	1e-4, 3e-4, 0.001, 0.003, 0.01, 0.03, 0.1, 0.3	0.01, 0.03, 0.1, 0.3, 1, 3, 10

our experiment to train the models and compute the training losses.

We used binary entropy loss (with sigmoid) for MNIST and CURVES, and squared error loss for FACES. The above settings largely mimic the settings in (Martens, 2010; Martens & Grosse, 2015; Botev et al., 2017; ?; Ren & Goldfarb, 2021b). Since we primarily focused on optimization rather than generalization in these tasks, we also did not include L_2 regularization or weight decay.

In order to obtain Figure 7, we first conducted a grid search on the learning rate (lr) and damping value based on the criteria of minimizing the training loss. The ranges of the grid searches used for the algorithms in our tests are specified in Table 6.

The best hyper-parameter values determined by our grid searches are listed in Table 5.

Table 7: Hyper-parameters (learning rate, damping) used to produce Figure 7

Name	MNIST	FACES	CURVES
MBF	(1e-5, 3e-4) \rightarrow 51.49	(1e-6, 0.003) \rightarrow 5.17	(1e-5, 3e-4) \rightarrow 55.14
KFAC	(0.003, 0.3) \rightarrow 53.56	(0.1, 10) \rightarrow 5.55	(0.01, 1) \rightarrow 56.47
Shampoo	(3e-4, 3e-4) \rightarrow 53.80	(3e-4, 3e-4) \rightarrow 7.21	(0.001, 0.003) \rightarrow 54.86
Adam	(3e-4, 1e-4) \rightarrow 53.67	(1e-4, 1e-4) \rightarrow 5.55	(3e-4, 1e-4) \rightarrow 55.23
SGD-m	(0.003, -) \rightarrow 55.63	(0.001, -) \rightarrow 7.08	(0.01, -) \rightarrow 55.49

B.3. Experiment Settings for the CNN Problems

The ResNet32 model refers to the one in Table 6 of (He et al., 2016), whereas the VGG16 model refers to model D of (Simonyan & Zisserman, 2014), with the modification that batch normalization layers were added after all of the convolutional layers in the model. For all algorithms, we used a batch size of 128 at every iteration.

We use weight decay for all the algorithms that we tested, which is related to, but not the same as L_2 regularization added to the loss function, and has been shown to help improve generalization performance across different optimizers (Loshchilov & Hutter, 2019; Zhang et al., 2019b). The use of weight decay for MBF and Shampoo is described in Algorithm 2 and Algorithm 3, respectively, and is similarly applied to SGD-m, Adam, and KFAC.

For MBF, we set $\lambda = 0.003$. We also tried values around 0.003 and the results were not sensitive to the value of λ . Hence, λ can be set to 0.003 as a default value. For KFAC, we set the overall damping value to be 0.03, as suggested in the implementation in <https://github.com/alecwangcq/KFAC-Pytorch>. We also tried values around 0.03 for KFAC and confirmed that 0.03 is a good default value.

In order to obtain Figure 6, we first conducted a grid search on the initial learning rate (lr) and weight decay (wd) factor based on the criteria of maximizing the classification accuracy on the validation set. The range of the grid searches for the algorithms in our tests are specified in Table 8.

The best hyper-parameter values, and the validation classification accuracy obtained using them, are listed in Table 9.

Table 8: Grid of hyper-parameters for CNN problems

Algorithm	learning rate	weight decay γ
SGD-m	3e-5, 1e-4, 3e-4, 0.001, 0.003, 0.01, 0.03, 0.1, 0.3, 1	0.01, 0.03, 0.1, 0.3, 1, 3, 10
Adam	1e-6, 3e-6, 1e-5, 3e-5, 1e-4, 3e-4, 0.001, 0.003, 0.01, 0.03	0.01, 0.03, 0.1, 0.3, 1, 3, 10
Shampoo	3e-5, 1e-4, 3e-4, 0.001, 0.003, 0.01, 0.03, 0.1	0.01, 0.03, 0.1, 0.3, 1, 3, 10
MBF	1e-6, 3e-6, 1e-5, 3e-5, 1e-4, 3e-4, 0.001, 0.003	0.01, 0.03, 0.1, 0.3, 1, 3, 10
KFAC	3e-6, 1e-5, 3e-5, 1e-4, 3e-4, 0.001, 0.003, 0.01, 0.03	0.01, 0.03, 0.1, 0.3, 1, 3, 10

Table 9: Hyper-parameters (initial learning rate, weight decay factor) used to produce Figure 6 and the average validation accuracy across 5 runs with different random seeds shown in Figure 6

Name	CIFAR-10 + ResNet32	CIFAR-100 + VGG16	SVHN + VGG11
MBF	(1e-4, 3) \rightarrow 93.42%	(3e-5, 10) \rightarrow 74.80%	(0.001, 0.3) \rightarrow 96.59%
KFAC	(0.003, 0.1) \rightarrow 93.02%	(0.001, 0.3) \rightarrow 74.38%	(0.003, 0.1) \rightarrow 96.37%
Shampoo	(0.01, 0.1) \rightarrow 92.97%	(0.001, 0.3) \rightarrow 73.37%	(0.003, 0.1) \rightarrow 96.15%
Adam	(0.003, 0.1) \rightarrow 93.34%	(3e-5, 10) \rightarrow 72.95%	(3e-4, 1) \rightarrow 96.34%
SGD-m	(0.1, 0.01) \rightarrow 93.23%	(0.03, 0.01) \rightarrow 73.99%	(0.03, 0.01) \rightarrow 96.63%

B.4. Additional numerical results

Sensitivity to Hyper-parameters:

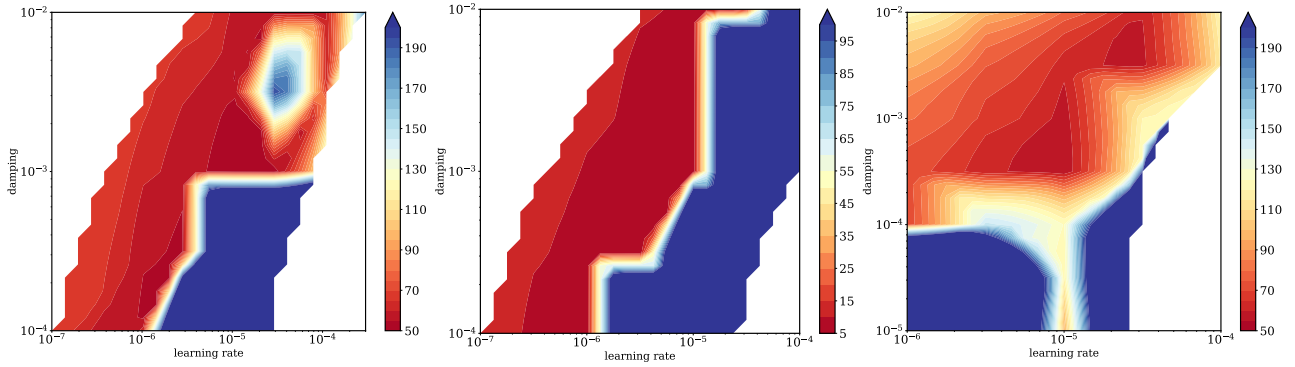


Figure 8: Landscape of loss w.r.t hyper-parameters (i.e. learning rate and damping). The left, middle, right columns depict results for MNIST, FACES, CURVES, which are terminated after 500, 2000, 500 seconds (CPU time), respectively.

Training and testing plots: For completeness, we report in Figures 9 and 10 both training and testing performance of the results plotted in Figures 6 and 7 in the main manuscript.

On the effect of the update frequencies T_1, T_2 : We also explored the effect of the update frequencies T_1, T_2 of the mini-block preconditionners as described in Algorithm 2. To be more specific, we tuned the learning rate for some combinations of T_1, T_2 as described in Figure 11. Comparing the performance of different configurations in Figure 11, we can see that the effect of the frequencies T_1, T_2 on the final performance of MBF is minimal and the configurations $T_1, T_2 = (1, 20)$, $T_1, T_2 = (2, 25)$ seem to yield the best performance in terms of process time for autoencoder problems.

B.5. More on MBF Motivation

As mentioned in the main manuscript, we include here additional examples that illustrate that most of the weight in the inverse of the empirical FIM resides in the mini-blocks used in MBF. For convolutional layers, we trained a simple convolutional neural network, Simple CNN on Fashion MNIST (Xiao et al., 2017). The model is identical to the base model

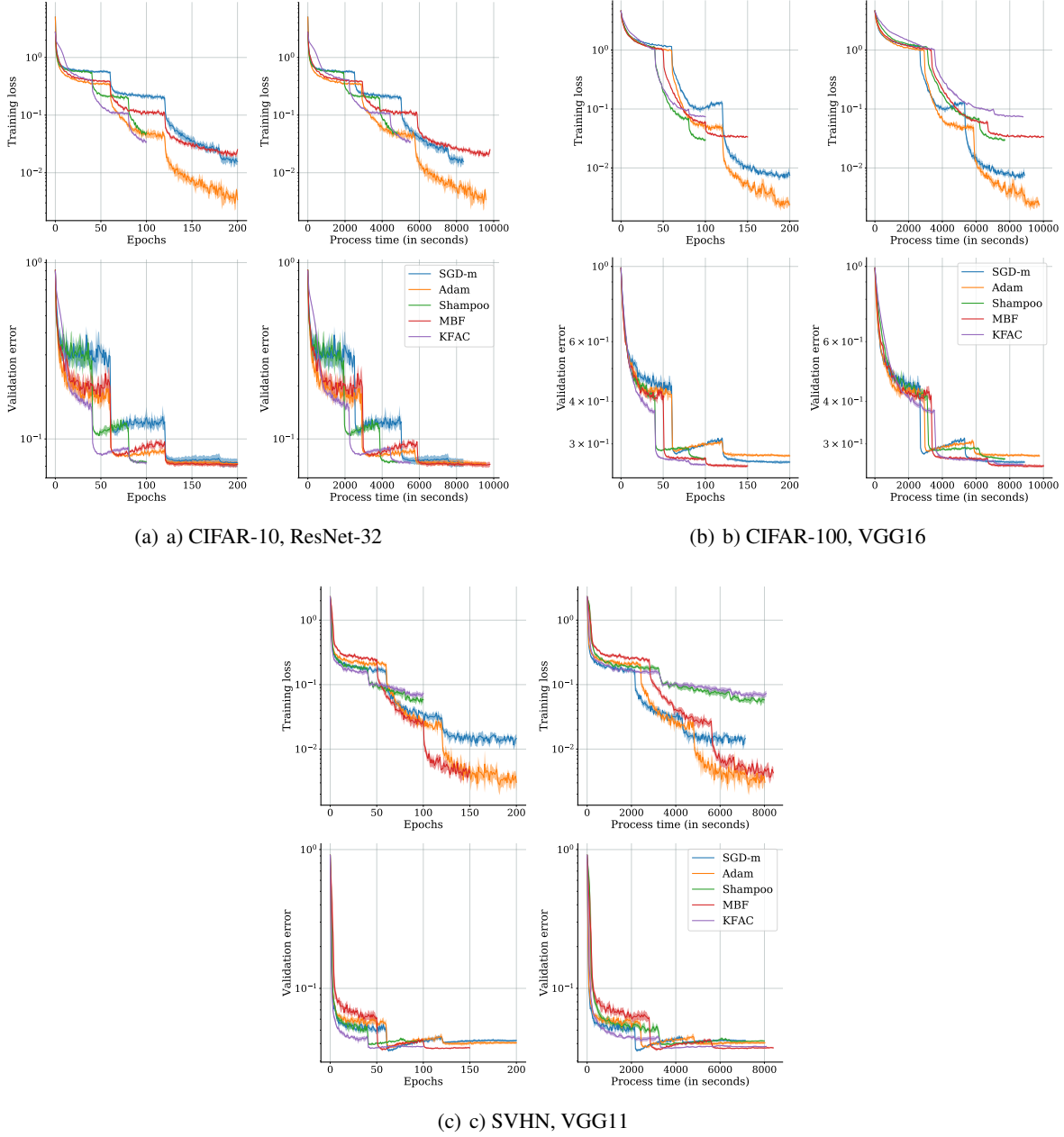
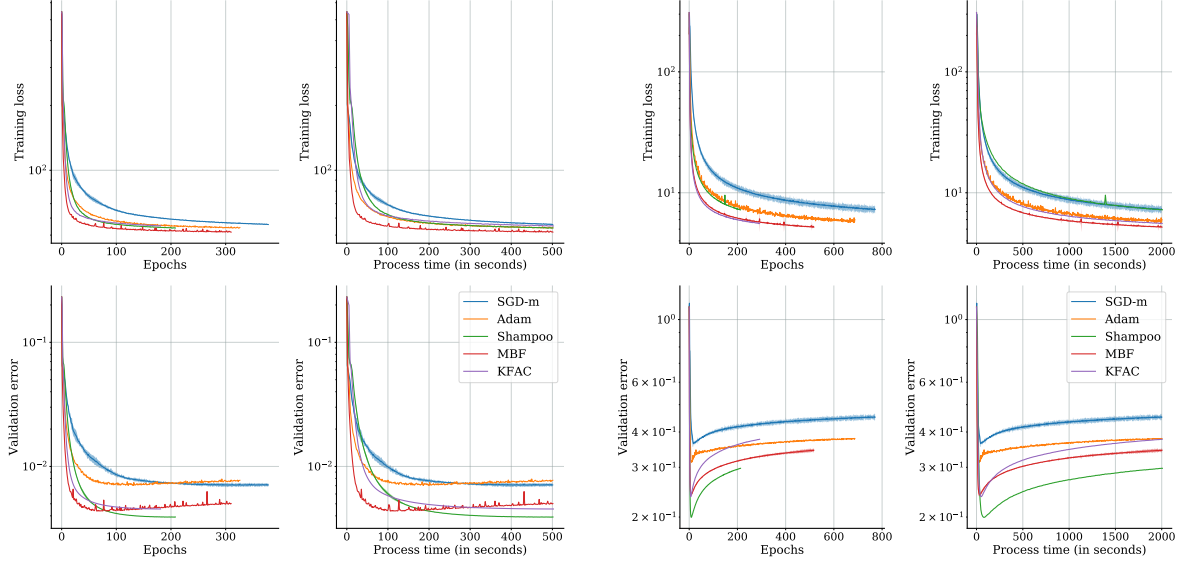


Figure 9: Training and testing performance of MBF, KFAC, Shampoo, Adam, and SGD-m on three CNN problems.

described in (Shallue et al., 2019). It consists of 2 convolutional layers with max pooling with 32 and 64 filters each and 5×5 filters with stride 1, “same” padding, and ReLU activation function followed by 1 fully connected layer. Max pooling uses a 2×2 window with stride 2. The fully connected layer has 1024 units. It does not use batch normalization.

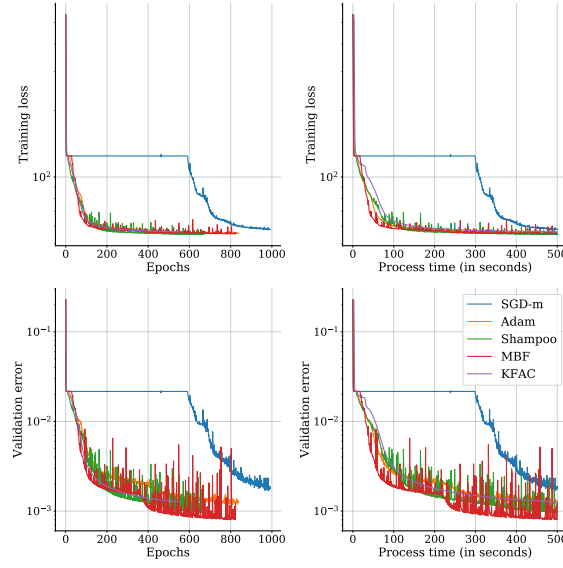
Figure 12 shows the heatmap of the absolute value of the inverse empirical FIM corresponding to the second convolutional layer for example channels 1, 16 and 32, which all use 64 filters of size 5×5 (thus 64 mini-blocks of size 25×25 per channel). One can see that the mini-block (by filter) diagonal approximation is reasonable.

As mentioned in the manuscript, we illustrate the mini-block structure of the FIM on a 7-layer (256-20-20-20-20-10) feed-forward DNN using tanh activations, partially trained (after 50 epochs using SGD-m) to classify a 16×16 down-scaled version of MNIST that was also used in (Martens & Grosse, 2015). Figure 13 shows the heatmap of the absolute value



(a) MNIST autoencoder

(b) FACES autoencoder



(c) CURVES autoencoder

Figure 10: Training and testing performance of MBF, KFAC, Shampoo, Adam, and SGD-m on three autoencoder problems.

of the inverse empirical FIM for the second fully connected layers (including bias). One can see that the mini-block (by neuron) diagonal approximation is reasonable.

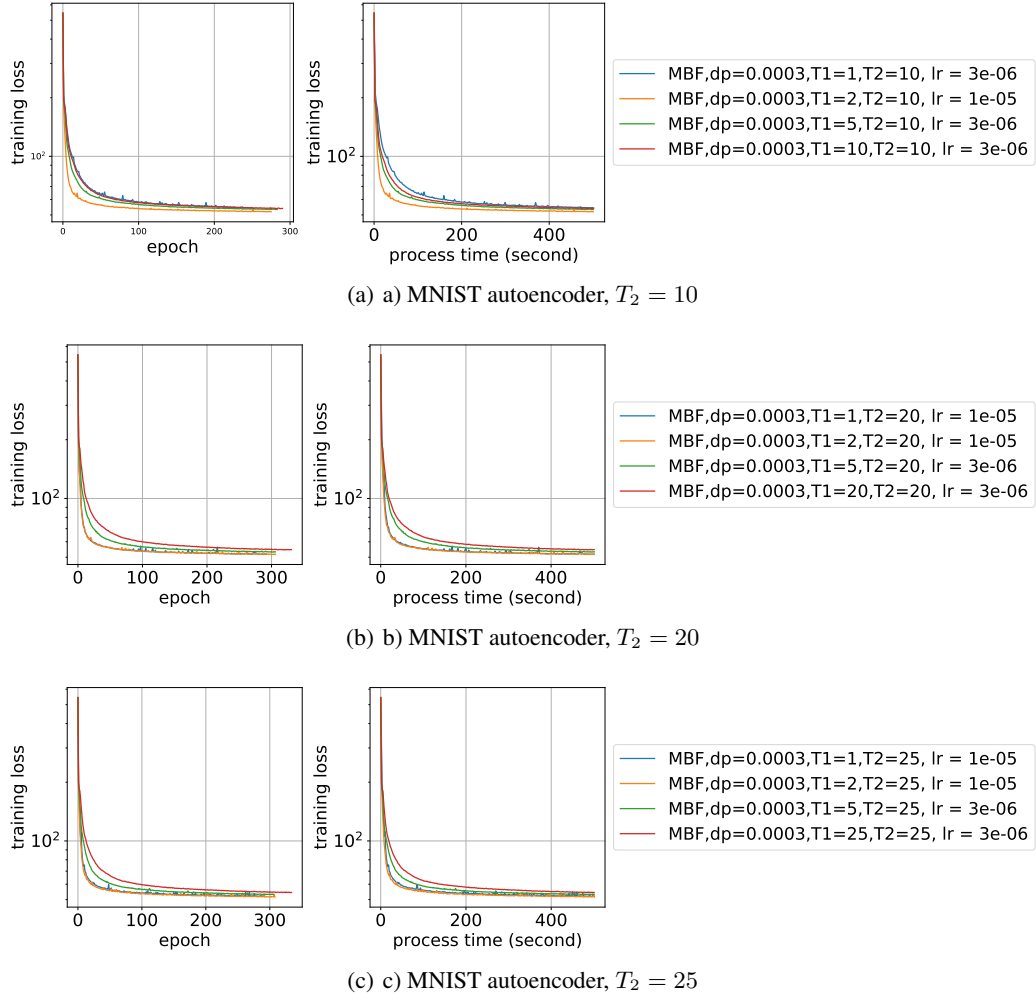
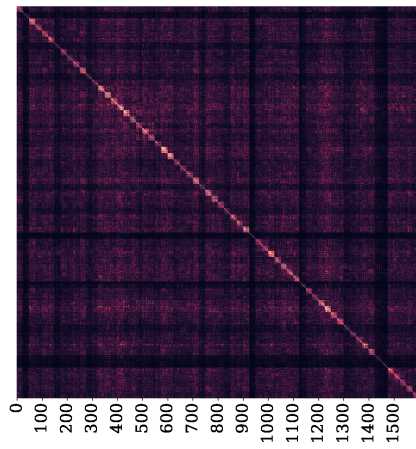
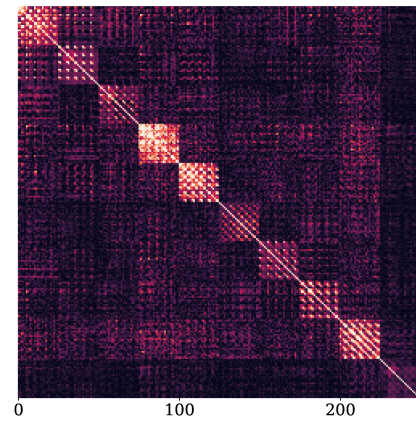


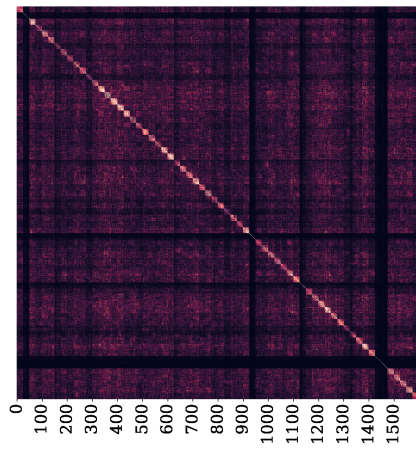
Figure 11: Training performance of MBF on MNIST autoencoder problems for some combinations of T_1, T_2 .



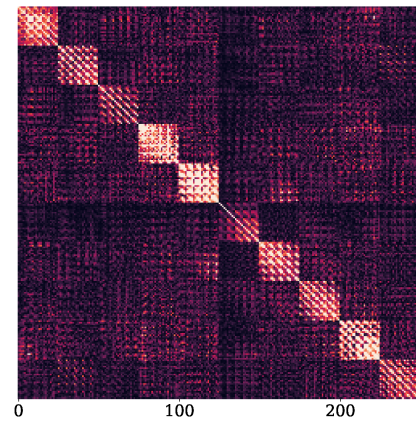
(a) Absolute inverse FIM for channel 1



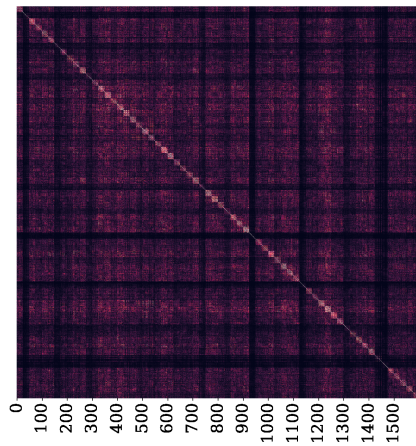
(b) Zoom on the 20th to 30th blocks



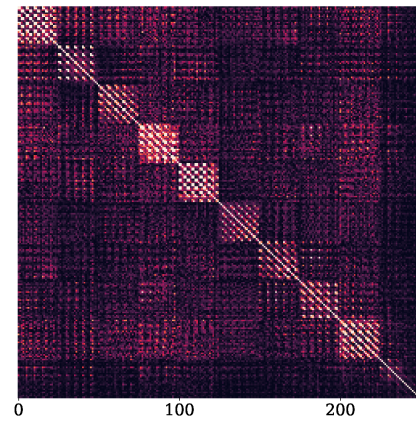
(c) Absolute inverse FIM for channel 16



(d) Zoom on the 20th to 30th blocks



(e) Absolute inverse FIM for channel 32



(f) Zoom on the 20th to 30th blocks

Figure 12: Absolute inverse of the empirical FIM after 10 epochs for the second convolutional layer of the Simple-CNN.

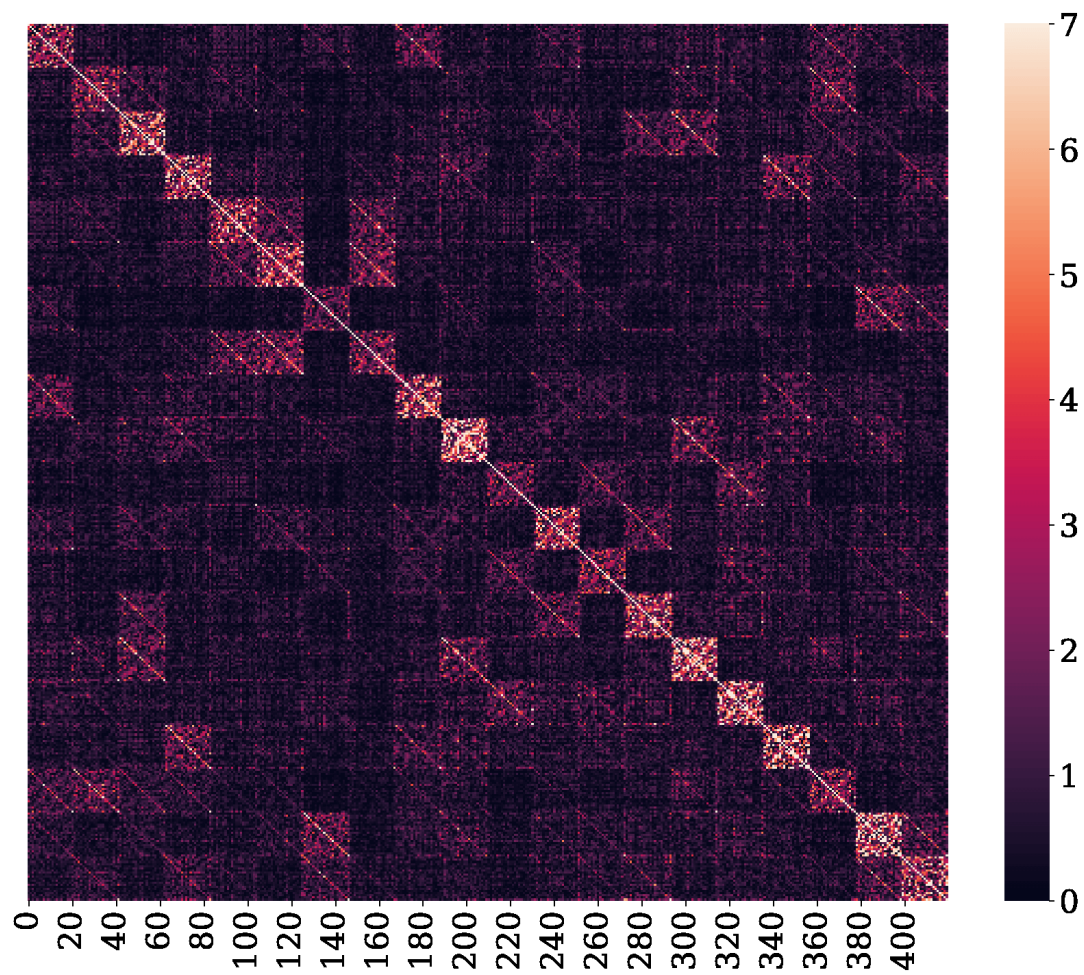


Figure 13: Absolute inverse FIM, second fully connected layer 20-20